A layers-overlapping strategy for robotic wire and arc additive manufacturing of multi-layer multi-bead components with homogeneous layers

Li, Yongzhe; Han, Qinglin; Zhang, Guangjun; Horvath, Imre

DOI
10.1007/s00170-018-1786-3

Publication date
2018

Document Version
Accepted author manuscript

Published in
International Journal of Advanced Manufacturing Technology

Citation (APA)
Li, Y., Han, Q., Zhang, G., & Horvath, I. (2018). A layers-overlapping strategy for robotic wire and arc additive manufacturing of multi-layer multi-bead components with homogeneous layers. *International Journal of Advanced Manufacturing Technology*, *96*, 3331-3344. https://doi.org/10.1007/s00170-018-1786-3

A layers-overlapping strategy for robotic wire and arc additive manufacturing of multi-layer multi-bead components with homogeneous layers

Yongzhe Li[a,b], Qinglin Han[a], Guangjun Zhang[a], Imre Horváth[b]

a: State Key Laboratory of Advanced Welding and Joining, Harbin Institute of Technology, 150001, Harbin, China

b: Faculty of Industrial Design Engineering, Delft University of Technology, 2628 CE, Delft, The Netherlands

Corresponding author: Guangjun Zhang.

Postal address: State Key Laboratory of Advanced Welding and Joining, Harbin Institute of Technology, No.92, West Da-Zhi Street, Harbin, Heilongjiang, 150001, China.

Tel.: +86 451 86415537; Fax: +86 451 86415537.

E-mail address: zhanggj@hit.edu.cn.

Author name: Yongzhe Li

E-mail address: y.li-8@tudelft.nl

Author name: Qinglin Han

E-mail address: hanqinglin2014@163.com

Author name: Imre Horváth

E-mail address: I.Horvath@tudelft.nl

A layers-overlapping strategy for robotic wire and arc additive manufacturing of multi-layer multi-bead components with homogeneous layers

Yongzhe Li[a,b], Qinglin Han[a], Guangjun Zhang[a], Imre Horváth[b]

a: State Key Laboratory of Advanced Welding and Joining, Harbin Institute of Technology, 150001, Harbin, China

b: Faculty of Industrial Design Engineering, Delft University of Technology, 2628 CE, Delft, The Netherlands

Abstract

Robotic wire and arc additive manufacturing (WAAM) systems are required to provide predictable and efficient operations to fabricate solid metallic parts with high morphological fidelity and geometric accuracy. Since the metallic parts are fabricated based on a layer-by-layer principle, the interactions between the neighboring beads and layers strongly influence the geometric accuracy of the fabricated part. The layers-overlapping process has been studied and a traditional layers-overlapping model (T-LOM) has been published in the literature. This paper proposes a layers-overlapping strategy (LOS), based on which a revised layers-overlapping model (R-LOM) was proposed for the fabrication of multi-layer multi-bead (MLMB) components with homogeneous layers. A mathematical model for layers-overlapping is presented, which considers the material shortage areas at the edges of the layers. This is important since the material shortage areas result in a situation that the component width is smaller than the expected value. In addition, they will be accumulated when multiple layers are overlapped through normal unidirectional parallel (NUP) paths. The proposed LOS addresses two aspects: (i) the deposition amount of the first bead and the last bead in the lap layers should be increased, and (ii) the deposition position of the first bead and the last bead in the lap layers should be moved towards the edges with a given offset distance. Validation experiments were designed and conducted to test the proposed concepts and models. The experimental results indicated that (i) the R-LOM enables the MLMB components to achieve the expected width and (ii) for components deposited with NUP paths, the R-LOM eliminates the effect of accumulation of material shortage areas on the first bead and increases the surface flatness.

Keywords: additive manufacturing; gas metal arc welding; multi-layer multi-bead components; layers-overlapping model

Abbreviations used in the text

Abbr.	Term/Phase
WAAM	wire and arc additive manufacturing
T-LOM	traditional layers-overlapping model
LOS	layers-overlapping strategy
MLMB components	multi-layer multi-bead components
R-LOM	revised layers-overlapping model
$B(i,j)$	the j^{th} bead belonging to the i^{th} layer
EB	elementary bead
NUP paths	normal unidirectional parallel paths
IRUP paths	interlayer-reverse unidirectional parallel paths

CUP paths	curved unidirectional parallel paths
FoS	flatness of the surface
DEH	deviation from the expected height

Please print all figures in grayscale.

1. Introduction

As a low-cost, energy- and time-efficient approach for manufacturing of metallic parts, wire and arc additive manufacturing (WAAM) is getting more and more attention in research nowadays. Various research related to WAAM technologies and implementations of WAAM systems have been reported in the literature, regarding (i) fundamental principles [1], (ii) mechanical performance of the fabricated part [2], and (iii) manufacturing processes [3] etc.

Automatic/robotic WAAM increases the efficiency of manufacturing and reduces the involved human intervention [4]. Robotic WAAM systems are required to provide not only predictable and efficient operations but also high morphological fidelity and geometric accuracy of the fabricated parts [5]. A slight difference between the geometries of the CAD model and the fabricated part might invalidate the preplanned manufacturing parameters [6]. Therefore, many approaches have been proposed to increase the geometric accuracy of the fabricated parts, e.g. (i) geometry improvement based on the temperature field control [7], (ii) process control based on passive-vision sensing [8,9], and (iii) integrated processing with additive and subtractive manufacturing [10,11]. It can be concluded that relatively high accuracy has been achieved regarding the fabrication of single-walled parts. As a contrast, the accuracy of multi-layer multi-bead (MLMB) components is still relatively low and the surface finish of them is usually insufficient. These facts indicate that more research attention should be given to the fabrication of MLMB components.

MLMB components are fabricated on a bead-by-bead and layer-by-layer basis. Different to the thin-walled components, which contain only one bead in a layer, a MLMB component is composed of a number of layers with multiple straight or curved weld beads. Accordingly, the interactions between the neighboring beads and layers strongly influence the geometric accuracy of MLMB components. The overlapping model of weld beads is an important technological issue and has been addressed in the literature. Aiyiti et al. described the cross-sectional profile of a

single weld bead as a circular arc and developed a simple overlapping model for adjacent weld beads [12]. Cao et al. used sine function to model the cross-sectional profile of a single weld bead. They found that the optimal step-over rate (central distance of adjacent beads over the width of a single weld bead) is 63.66% [13]. In addition, a symmetric parabola model was used to represent the cross-sectional profile of a single weld bead in [14] and [15]. They considered the step-over rate as 66.66% and 73.8%, respectively. Recently, Li et al. proposed that the spreading effect of molten weld beads should be taken into consideration of the beads-overlapping model and an enhanced beads-overlapping model was reported [16]. Based on the findings from the literature, most of the related work focused on the mathematical formulation of beads-overlapping process in a single layer. However, the layers-overlapping process is also an important aspect of research for WAAM, but is rarely addressed. Therefore, the layers-overlapping process of MLMB components needs a detailed mathematical specification to support the design and manufacturing processes.

Various layers-overlapping strategies are applied in the practice of fabrication of MLMB components, e.g. alternating the layers by 90 degrees or 180 degrees [17]. As a simplified case to start the primary research concerning the mathematical formulation of the layers-overlapping process, this paper focuses on MLMB components with homogeneous layers. This type of MLMB components will be referred to as cuboid components in the rest of this paper. Every layer of a cuboid component contains an equal number of homogeneous weld beads, which are deposited with an equal center distance between adjacent beads. In addition, multiple layers are overlapped with the same deposition direction, and every weld bead in a lap layer is coaxial to the weld bead underneath. This results in the same cross-sectional profile of the layers in the component. A cuboid component is an idealization of an MLMB component with complex structure, e.g. the thick-walled parts.

The content of this paper is organized as follows: the layers-overlapping process is analyzed and some limitations of the traditional layers-overlapping model (T-LOM) are identified in Section 2. Then, the details of a layers-overlapping strategy (LOS) for fabrication of cuboid components are presented in Section 3. In Section 4, three validation experiments are reported, which were designed and conducted to verify (i) the limitations of the T-LOM, (ii) the proposed LOS and (iii) the revised layers-overlapping model (R-LOM) concerning the LOS. The conclusions of the

completed research and the planned future research are discussed in Section 5.

2. The process of layers-overlapping in WAAM

2.1 The basic model of a layer

Our investigation was based on the following assumptions: (i) As suggested in [14] and [15], the basic profile of a single weld bead is considered as a symmetrical parabola model. (ii) If the different heat dissipation conditions at different positions of an cuboid component are neglected, the basic model of single weld beads is assumed to be unchanged during the overlapping process. It means that homogeneous beads are overlapped. (iii) As a simplification, the one by one deposition order of weld beads in a single layer is supposed to be from one side to another in the layers-overlapping process considered in this research. (iv) Furthermore, considering the observations presented in [15]: it is impossible to achieve an ideal flat surface on the joint of adjacent weld beads if a steady increase of layers is to be expected. The upper surface of a layer is considered as a waved shape.

Based on these assumptions, a basic model of the cross-sectional profile of a layer is constructed, as shown in Fig. 1. According to their order of deposition, the weld beads included in a layer are identified as (i) the first bead, (ii) the lap bead(s) and (iii) the last bead. The segment between the center of the first bead and the center of the last bead in a layer is referred to as 'the main body of the layer', while the left half of the first bead and the right half of the last bead are referred to as 'the edges of the layer'.

According to the basic model shown in Fig. 1, the distance between the centers of adjacent beads is $d = aw$, where w is the width of a single bead, and a is the step-over rate between adjacent

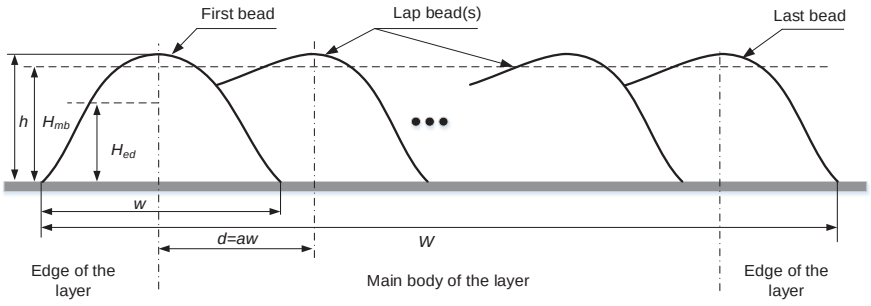

Fig. 1 The basic model of a layer

beads ($0.5 < a < 1$). The width of the layer, W, which is defined as the distance from the left-most point of the first bead (the left toe of the first bead) to the right-most point of the last bead (the right toe of the last bead) of the layer, is calculated so as:

$$W = aw(n-1) + w \tag{1}$$

where n is the number of weld beads in the layer and $n \geq 2$.

The average height of the main body of the layer, H_{mb}, is calculated as:

$$\mathrm{H}_{mb} = \frac{\frac{2}{3}wh}{d} = \frac{2h}{3a} \tag{2}$$

where h is the height of a single weld bead. In addition, the average height of the edges of the layer is calculated as:

$$\mathrm{H}_{ed} = \frac{\frac{1}{3}wh}{\frac{1}{2}w} = \frac{2h}{3} \tag{3}$$

Based on a comparison between Equations (2) and (3), it can be seen that the average height of the edge of the layer is smaller than the average height of the main body of the layer since $a < 1$.

2.2 Limitation of the T-LOM

In the cuboid components, a lap layer is typically deposited on the top of the previous layer by the T-LOM so as that the deposition position of each bead in the lap layer should be in accordance with the center of the bead below. Based on the principle, the schematic diagram of the T-LOM is shown in Fig. 2. As analyzed in the basic model of a layer, the layer's edge is lower than the layer's main body. When two layers are overlapped, material shortage areas are generated at both edges of the lap layer. In addition, the material shortage areas might be accumulated, when multiple layers are overlapped, as identified in Fig. 2. According to the T-LOM, the accumulation of material shortage results in a phenomenon that the height of the edges is getting lower and lower with regard to the main body when the number of layer increases.

However, the design of the manufacturing parameters for the cuboid components should consider the height of the main body as the height of the layer, i.e. $H = H_{mb}$, since the number of weld beads contained in a layer depends on the morphology of the target component. Accordingly, if the

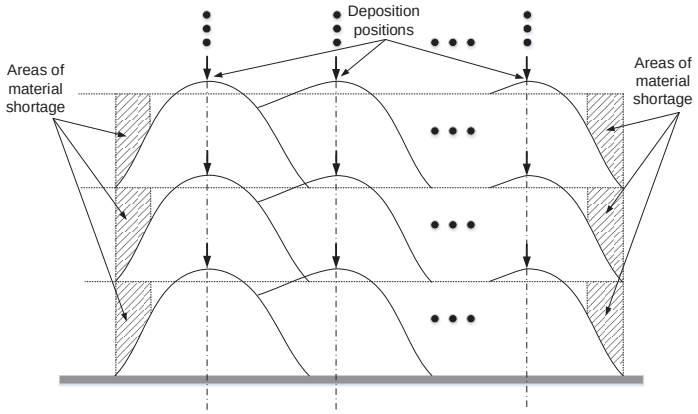

Fig. 2 The schematic diagram of the layers-overlapping process according to the T-LOM

robot used in the WAAM system follows the preplanned deposition paths, the nozzle-to-plate distance (the distance between the weld gun and the component) for deposition of the first bead and the last bead of lap layers will increase as the number of layer increases. Evidently, the increased nozzle-to-plate distance deviates from a planned value and may prevent the protection of the shielding gas coming out from the weld gun and prolong the length of the arc. Both situations may produce failures in the fabricated component, e.g. porosities. The robotic manufacturing process has to be terminated.

According to the basic model, the accumulation of material shortage areas in the T-LOM of cuboid components is caused by the height difference between the layer's edge and the layer's main body. This problem does not attract research attention in the work related to the single-walled parts. This is because that the single-walled parts do not have the main body in their layers. Thus, the layer's height equals the height of the layer's edge, which is $2h/3$ in the proposed model. However, this issue should be addressed to fabricate cuboid components and the T-LOM should be revised.

3. Revising the T-LOM with a LOS

To achieve a stable layers-overlapping process, the problem of the material shortage area should be solved. The first requirement is that the edge of a lap layer should increase with the same height as the main body of the lap layer has reached. In addition, the surface shape of the lap layer should be the same as the surface of the supporting layer to realize a repetitive overlapping process. Towards these ends, the morphological effect of the first bead in the second layer was considered as a demonstrative case to give attention to the edges of the layer from the viewpoint of material

shortage. For the sake of simplicity, $B(i,j)$ was used to represent the j^{th} bead belonging to the i^{th} layer.

The overlapping model of $B(2,1)$ is shown in Fig. 3. When $B(2,1)$ is deposited on the top of $B(1,1)$, the expected cross-sectional profile of $B(2,1)$ is $\widehat{\mathrm{BAG}}$. Since the step-over rate $a < 1$, the area $S_{BEC} > S_{DEF}$. The material shortage area generated between the two layers is calculated as:

$$S_{ms} = S_{BEC} - S_{DEF} \tag{4}$$

It was assumed that a weld bead $B(2,1)'$ is deposited on the top of $B(1,1)$, instead of $B(2,1)$. To achieve a steady increase of the layer, $B(2,1)'$ should fill the area S_{ABCDFG}. It means that $B(2,1)'$ has to be deposited with additional amount of material, which covers the amount of material shortage S_{ms}. The area of the cross-sectional profile of the assumed $B(2,1)'$ is calculated as follows:

$$S_{B(2,1)'} = S_{ABCD} + S_{AFG} = \frac{1+a}{3a}wh \tag{5}$$

If the first bead of the first layer deposited on the substrate is defined as the elementary bead (EB) of a cuboid component, the EB is considered as a reference to calculate the area of $B(2,1)'$. The area of an EB is calculated as follows:

$$S_{EB} = \frac{2}{3}wh \tag{6}$$

Therefore,

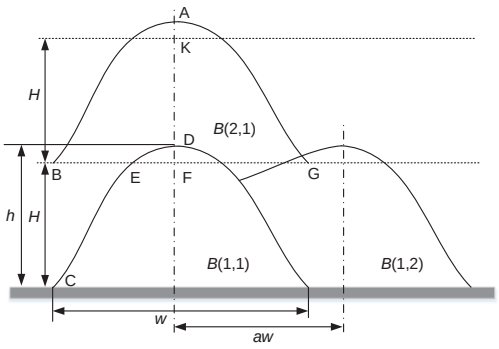

Fig. 3 The overlapping model of $B(2,1)$

$$\frac{S_{B(2,1)'}}{S_{EB}} = \frac{1+a}{2a} \tag{7}$$

The Equation (7) shows the relationship between the area of $B(2,1)'$ when it is required to cover the area of S_{ABCDFG}, and the area of the EB in the cuboid component. According to the basic model of a layer, the two edges are symmetric. The required deposition amount for the first bead in a lap layer is the same as that for the last bead. Therefore, Equation (7) in turn implies the relationship between the required deposition amount of the first bead and the last bead of lap layers, and that for the EB.

In addition, the shape of the first and last beads in the lap layers should also be considered. It can be seen in Fig. 3 that the area expected to be covered by $B(2,1)'$ is asymmetric, but the actual profile of $B(2,1)'$ is considered as a symmetrical parabola model. It entails that $B(2,1)'$ cannot fill the area of material shortage well, if $B(2,1)'$ is deposited in concentric with $B(1,1)$. To deal with this issue, $B(2,1)'$ should be deposited at the center of the expected area of $B(2,1)'$. It means that the deposition position of $B(2,1)'$ should move towards the edge of the layer with a specific offset distance, as shown in Fig. 4. The offset distance is calculated by the following formula:

$$d_o = \frac{w}{2} - \frac{\frac{1}{2}S_{B(2,1)'}}{H} = \frac{1-a}{4}w \tag{8}$$

where: a refers to the step-over rate, and w is the width of the EB.

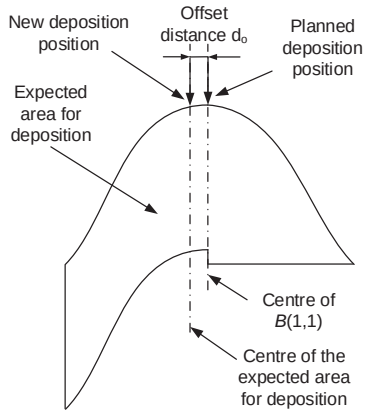

Fig. 4 Change of the deposition position of $B(2,1)$

To summarize the above discussed matters, the LOS implies two principles: (i) the deposition amount of the first bead and the last bead of lap layers should be increased, and (ii) the deposition positions of the first bead and the last bead of lap layers should be moved towards the edge with an offset distance.

The proposed LOS is used to revise the T-LOM. The revised LOM (R-LOM) supports the planning of the manufacturing parameters for fabrication of cuboid components by WAAM. Fig. 5 shows the work-flow of the planning software to generate fabrication parameters for a cuboid component. The planning is made according to the principles of the proposed LOS. It can be seen that both the welding parameters and the trajectory parameters should be purposefully modified. Validation experiments were conducted in order to prove that the R-LOM indeed does what it is supposed to do in real-life situations. The next Section will summarize the completed experiments and reflect on the findings.

4. Experimental validation

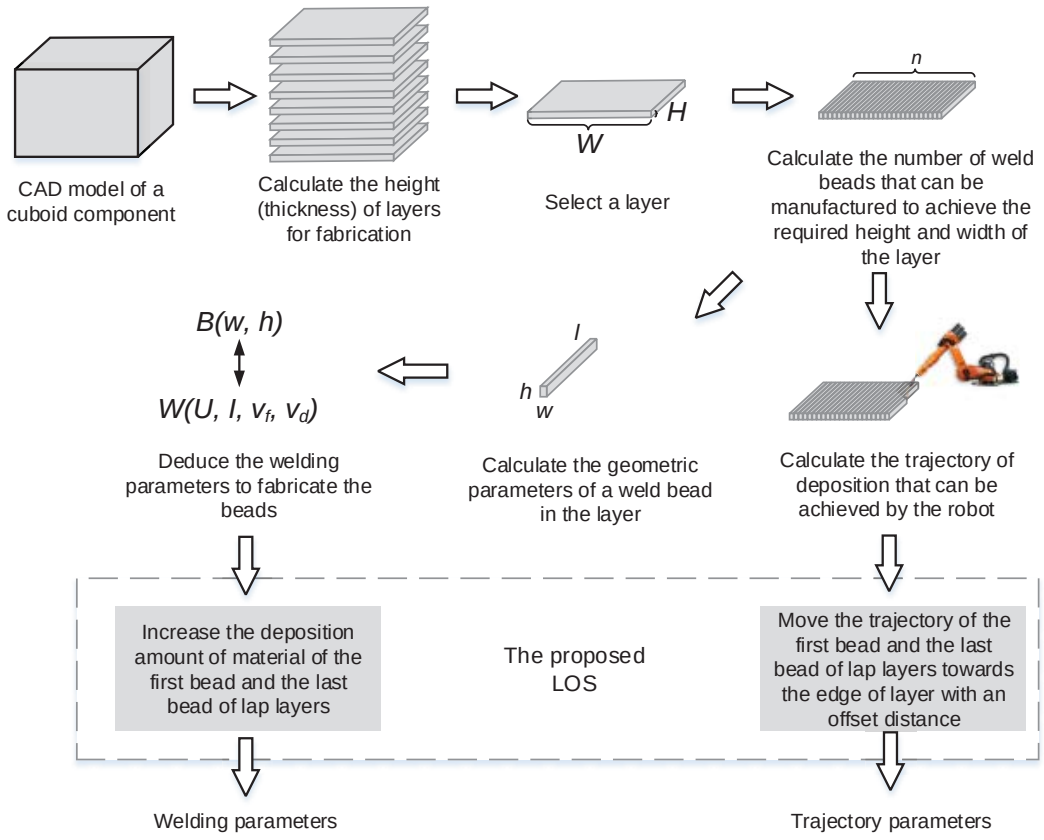

Fig. 5 The work-flow for planning the manufacturing parameters of a cuboid component

4.1 Setup of the experiments

The experiments were done by using a robot-based WAAM system implemented at the Harbin Institute of Technology. The functional architecture of the system is shown in Fig. 6. It includes a Motorman HP20D six-axis robot, a Panasonic YD-500FR welding machine with a YW-50KM wire feeding machine, a data acquisition card, a META SLS-050 V1 sensor, a manufacturing platform, and a personal computer. The accuracy of the measurement system was 0.05mm, while the accuracy of the motion system was 0.06 mm. The wire electrode used for deposition was copper coated steel wire with a composition of C (0.11%), Si (0.65%-0.95%), Mn (1.8%-2.1%), Ni (0.3%) and Cr (0.2%). The diameter of the fed wire was 1.2 mm. A mixture of Ar (95%) and CO_2 (5%) was used as the shielding gas with a flow rate of 18 L/min. The substrate material was Q235 with the size of 250 mm×100 mm×10 mm (length × width × height). In the experiments, the nozzle-to-plate distance was kept 12±0.3 mm in order to maintain a stable deposition process.

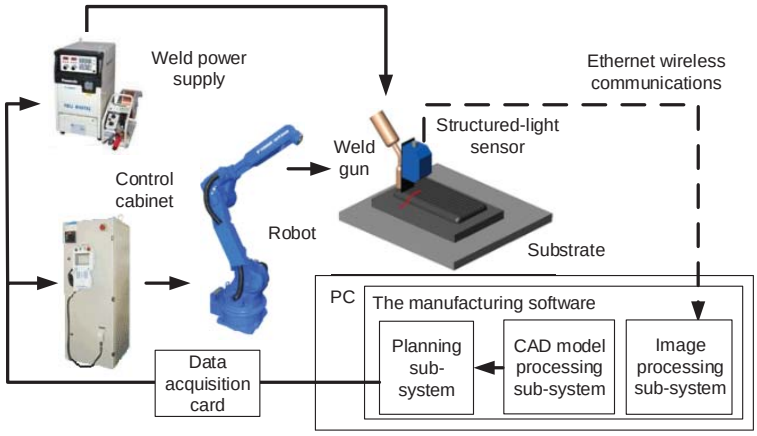

Fig. 6 Schematic diagram of the robotic-based WAAM system

The implemented manufacturing software in the personal computer was used for (i) processing the CAD models of the target components (ii) planning the manufacturing parameters, and (iii) processing the structured-light stripes aggregated from the sensor. The planned manufacturing parameters include (i) welding parameters and (ii) trajectory parameters. The trajectory parameters were sent to the robot control cabinet to control the motion of the robot, while the welding parameters were sent to the GMAW power supply unit. Both the robot control cabinet and the welding power supply unit were controlled so as to work in concert during the deposition process. When the deposition process of a weld bead or a layer was finished, the structured-light sensor

was used to detect the surface of the deposited bead or layer. In order to keep the experimental results consistent, same EBs were considered in the validation experiments. The manufacturing parameters to fabricate the EBs are shown in Table 1. The width and height of the EB were measured from the cross-section profile of a single weld bead, which was deposited on the substrate before the experiments.

Table 1 Manufacturing parameters used in the validation experiments

Manufacturing parameters (Unit)	Value
Wire feed rate (m/min)	3.73
Welding voltage (V)	22
Welding current (A)	150
Deposition speed for the EB (mm/s)	6
Width of the EB (mm)	7.327
Height of the EB (mm)	2.304
Step-over rate	0.738
Distance between the centers of adjacent beads (mm)	5.407
Height of a layer (mm)	2.081

If the influence of the deposition directions on the overlapping of adjacent weld beads is neglected, the order to deposit parallel paths in a layer can be either “from left to right” or “from right to left”. When these two strategies are applied in the context of multiple layers, two strategies of deposition paths were considered in the validation experiments, namely, (i) normal unidirectional parallel (NUP) path, and (2) interlayer-reverse unidirectional parallel (IRUP) path, as shown in Fig. 7. Compared to the NUP paths, the IRUP paths reverses the order of deposition of the weld beads in adjacent layers. These two path-planning strategies were considered in the experiments in order to compare the shape-forming processes of the first beads and the last beads.

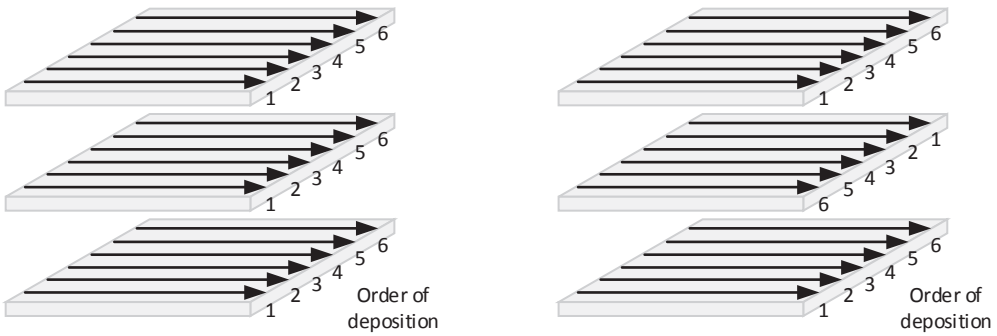

(a) (b)

Fig. 7 Two path-planning strategies applied in the validation experiments: (a) normal unidirectional parallel (NUP) path, (b) interlayer-reverse unidirectional parallel (IRUP) path

4.2 Validation experiments and results

4.2.1 Validation of the T-LOM

The first set of experiments was designed with the objective to test what the results of T-LOM are in practice. Another objective was to verify if the assumption regarding the material shortage areas in the proposed mathematical model is correct or not. To this end, two cuboid components were fabricated with the T-LOM. One component was fabricated with the NUP paths and another component was fabricated with the IRUP paths. Both cuboid components contained 10 layers and 6 weld beads in each of the layers. According to the Equation (1) and Equation (2), the height of the components was set to 20.810 mm, while the width of the components was set to 34.364 mm. The weld beads were deposited by using the manufacturing parameters in Table 1. After a layer was deposited, the system waited until the component cooled down to the room temperature. When this occurred, the deposition procedure for the next layer started.

The experimental results regarding the component with the NUP paths are presented in Fig. 8, while those for the component with the IRUP paths are presented in Fig. 9. In Fig. 8(b) and Fig. 9(b), the expected width and height of the cuboid components are presented. Thus, the expected cross-sectional profiles of the cuboid components are the quadrangles shaped by the dash lines.

It can be observed from the experimental results that material shortage areas were generated at both sides of the fabricated component. However, the situations of the sides were different. On the left side of the first component, accumulation of material shortage areas can be observed. That's why the material shortage area was mainly distributed on the top of the first bead of the 10^{th} layer. There was a small material shortage area generated at the side of the 2^{nd} and the 3^{rd} layers as well. The edges of the 4^{th} and above layers matched the expected position of the layer width very much. On the right side of the first component, the material shortage area was mainly generated at the side of the component. There was a slight difference between the total height of the last bead and that of the main body of the component. In addition, the main difference of the second component was that the situations of the material shortage areas at both edges were similar. Thus, both edges were lower than the height of the main body of the component. The material shortage areas can be found at both sides of the second component.

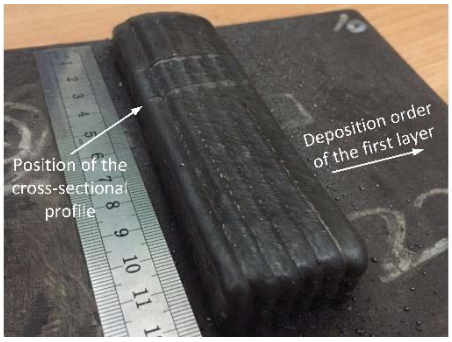

(a)

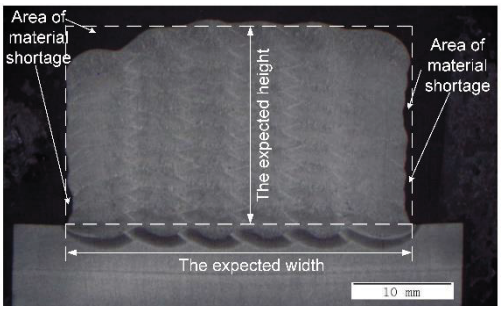

(b)

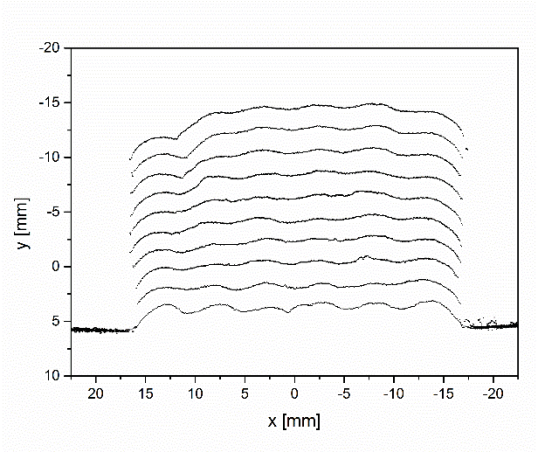

(c)

Fig. 8 The component fabricated based on the T-LOM and the NUP paths: (a) the overall view, (b) the cross-sectional profile, (c) layer surfaces

Based on the observed phenomenon, the first experiment validated the existence of the material shortage area when the T-LOM was applied to deposit cuboid components. More specifically, (i) the material shortage area caused by the first bead of a lap layer appeared on the top of the first bead and accumulated when multiple layers were overlapped, (ii) the material shortage area caused by the last bead of a lap layer mainly distributed at the side of the layer, and did not accumulate when multiple layers were overlapped, and (iii) depositing the weld beads by changing their deposition order in adjacent layers can alleviate the accumulation of material shortage areas caused by the first bead of the lap layers, however, it cannot eliminate the effect of material shortage areas generated at the side of the components.

To explain the phenomenon, the shapes of the positions where the first bead and the last bead of a lap layer are deposited are shown in Fig. 10. The main difference is that the last bead is deposited beside an already deposited neighboring bead, while there is no neighboring bead for the first bead in the same layer. Due to the fact that the shape of the position influences the force acting on the

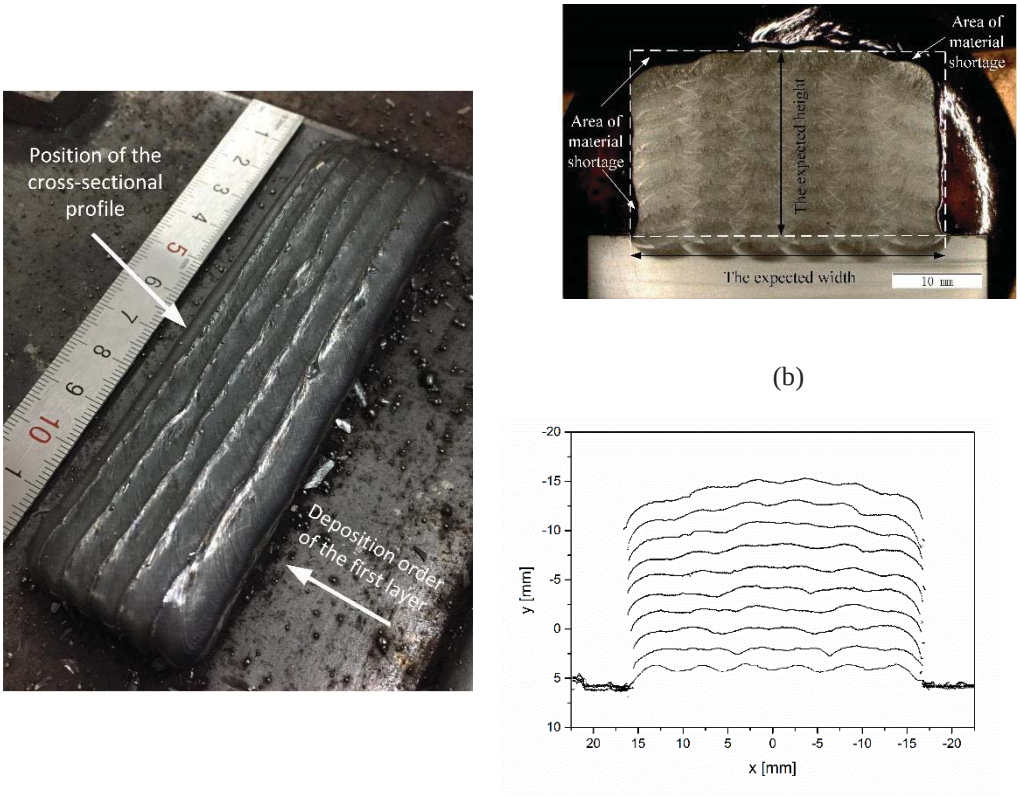

Fig. 9 The component fabricated based on the T-LOM and the IRUP paths: (a) the overall view, (b) the cross-sectional profile, (c) layer surfaces

weld bead, the observed phenomenon is explained from the following point of view: The weld bead remains in a liquid phase (as a weld pool) for a period of time when it is deposited on the already fabricated part (the solidified part). Then, the weld pool turns to the weld bead gradually. The force caused by the additional pressure of the curved liquid surface at the border of the weld pool influences the shape of the weld pool (and the weld bead as well). The additional pressure of a curved liquid surface is approximated by the following equation:

$$P_A = \frac{2\sigma}{r} \tag{9}$$

where: σ is the surface tension of the molten material, r is the radius of curvature of the curved liquid surface. If considered as a vector, the direction of $\boldsymbol{P_A}$ points from the curved liquid surface to the center of curvature.

As shown in Fig. 10(b), the additional pressure caused by the curved liquid surface at the left

border between the weld pool of the last bead and the solidified part enables the last bead to attach to the already deposited neighboring bead. However, the situation presented in Fig. 10(a) indicates that the additional pressure caused by the curved liquid surface at the right border between the weld pool of the first bead and the solidified part enables the first bead spread on the supporting layer. Accordingly, the first bead tends to be lower, while the last bead tends to be narrower. This is the reason why the area of the material shortage caused by the first bead mainly distributes on the top of the first bead, while that for the last bead mainly distributes at the side of the last bead.

4.2.2 Validation of the proposed LOS

The second set of experiments was designed to validate the feasibility of the LOS. Since the shapes of the positions for depositing the first bead and the last bead in a lap layer are different, the deposition processes of the beads were considered separately. In the experiment, two-layer cuboid components were deposited on the substrate and there were 6 weld beads in each layer. $B(2,1)$ and $B(2,6)$ were considered as reference cases to see the effectiveness of the LOS on them. The major (general) manufacturing parameters and experimental conditions for the second experiment were as the same as those presented in the first experiment, expecting the manufacturing parameters calculated based on the LOS.

To see the change with regard to the profile of the first bead, a comparative experiment was conducted to deposit $B(2,1)$ (i) with T-LOM, (ii) with increased deposition amount only, and (iii) with an increased deposition amount and a change of the deposition position. The increased

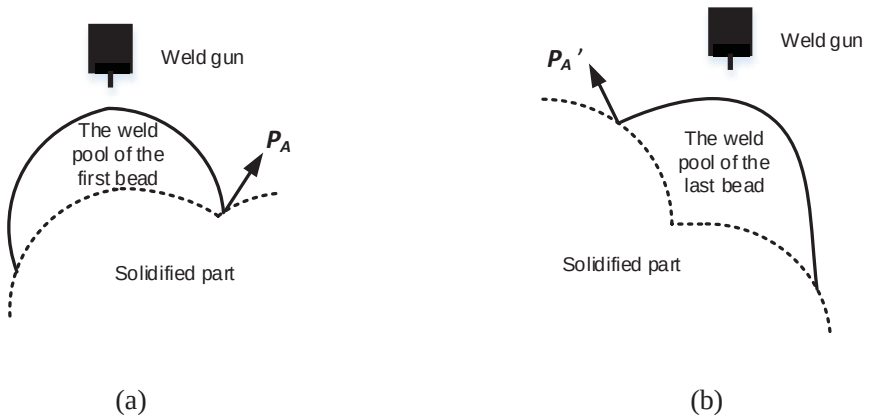

(a) (b)

Fig. 10 Shapes of the positions where the first bead and the last bead of a lap layer are deposited: (a) situation of the first bead, (b) situation of the last bead

deposition amount and the offset distance were calculated using Equations (7) and (8), respectively. To increase the deposition amount of a weld bead, the deposition speed of it was decreased. In the second experiment, the value of the decreased deposition speed was 5.10 mm/s, which was calculated by:

$$v_{d_{B(2,1)}} = \frac{2a}{1+a} v_{d_{EB}} \tag{10}$$

where $v_{d_{EB}}$ is the deposition speed for the elementary bead. The calculated offset distance was 0.480 mm.

The surface of the component in each situation was scanned by the structured-light sensor. The scanning was applied both before and after the deposition of $B(2,1)$. The light stripes which reflect the surface of the component were captured and combined to show the exact cross-sectional profile of $B(2,1)$. The experimental results of the comparative experiment are presented in Fig. 11. Fig. 11(a) shows a comparison between the profiles of $B(2,1)$ deposited with the T-LOM and with the increased deposition amount only. Based on the comparison in Fig. 11(a), it can be observed that the increased amount of material of $B(2,1)$ flowed to the valley between $B(1,1)$ and $B(1,2)$ when $B(2,1)$ was deposited exactly on the top of $B(1,1)$. Consequently, the center of $B(2,1)$ moved towards the joint of $B(1,1)$ and $B(1,2)$, instead of the material shortage area. This change had influence on the beads-overlapping process of the layer, since the

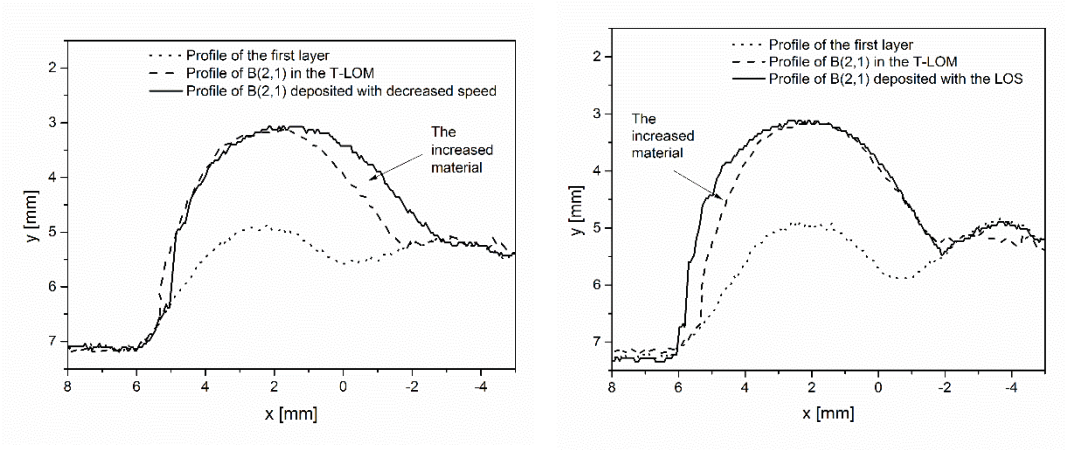

(a) (b)

Fig. 11 Experimental results: (a) the comparison between the profiles of $B(2,1)$ with T-LOM and with decreased deposition speed only, (b) the comparison between the profiles of $B(2,1)$ with T-LOM and with the proposed LOS

center distances between $B(2,1)$ and the rest of the beads in the second layer were changed. Oppositely, if the deposition position of $B(2,1)$ moved towards the edge (on the left side) with the calculated offset distance, the increased material of $B(2,1)$ filled up the material shortage area rather well, as shown in Fig. 11(b).

To see the change of the profile of the last bead, the profiles of $B(2,6)$ deposited (i) with the T-LOM and (ii) with the LOS were compared. The manufacturing parameters were the same as those calculated for deposition of $B(2,1)$. Fig. 12 shows a comparison between the profiles of $B(2,6)$ deposited in both situations. It can be observed from Fig. 12(a) that the $B(2,6)$ deposited with the T-LOM did not meet the requirement regarding the width of the layer, although the height of it was the same as the previously deposited neighboring bead (e.g. the $B(2,5)$). On the other hand, as presented in Fig. 12(b), the $B(2,6)$ deposited with the LOS reached the planned position of the width of the layer, while the height of it remained the same as the previously deposited neighboring bead (e.g. the $B(2,5)$).

Based on the second experiment, the feasibility of the LOS was validated. The proposed LOS enabled the coverage of material shortage areas generated at the edges of lap layers in the cuboid components. Therefore, the deficiencies of the T-LOM were overcome by using the proposed LOS, whose theoretical fundamentals have been discussed in Section 2.

4.2.3 Validation of the R-LOM

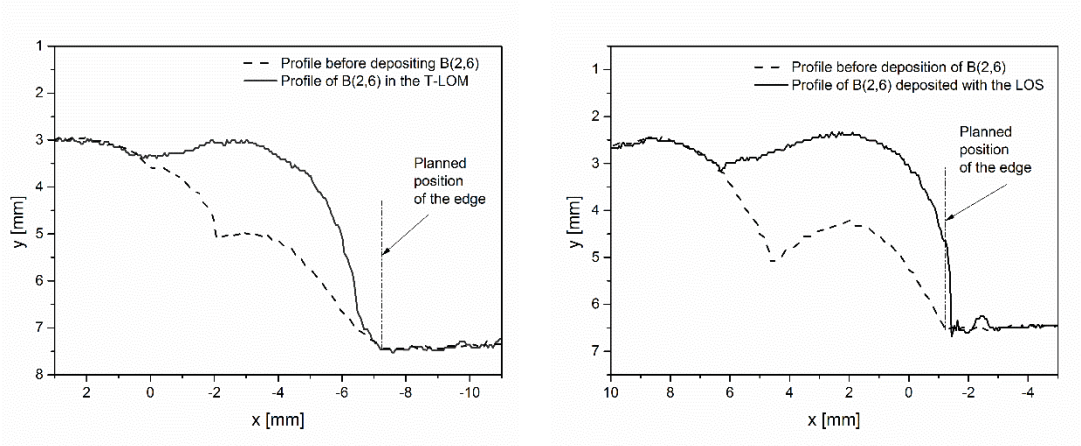

(a) (b)

Fig. 12 A comparison of the cross-sectional profile of $B(2,6)$ deposited with: (a) T-LOM, (b) with LOS

The third set of validation experiments was conducted to fabricate two cuboid components constructed with the R-LOM, in order to compare the performance of it with the T-LOM. The same path-planning strategies were applied to the two components. The manufacturing parameters and conditions for deposition of the cuboid components were the same as those used in the first experiment (presented in Section 4.2.1), excepting the manufacturing parameters for depositing the first bead and the last bead of the lap layers (2-10 layers). According to the LOS, the deposition speed for the first bead and last bead of the lap layers was set to 5.10 mm/s, while the offset distance was set to 0.480 mm, as the same as those calculated in the second experiment.

The component fabricated using the R-LOM and the NUP paths is shown in Fig.13, while the component fabricated using the R-LOM and the IRUP paths is shown in Fig.14. It can be seen that in both conditions, the components fabricated with the R-LOM fitted to the required areas (within

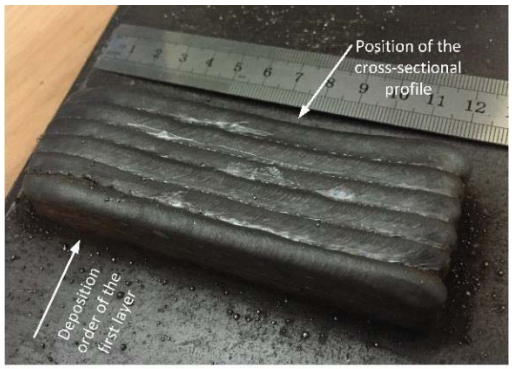

(a)

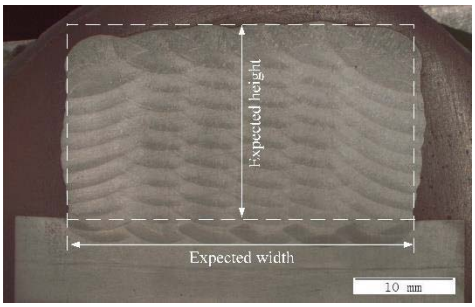

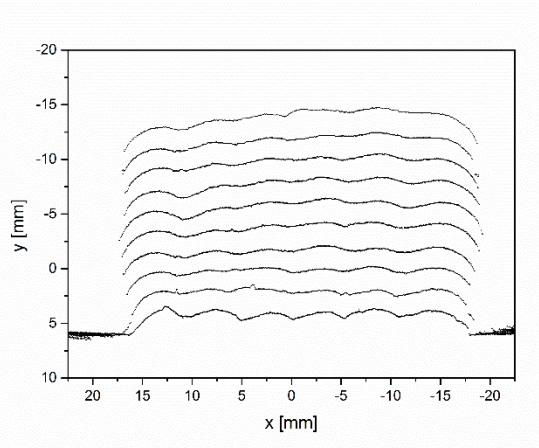

(b) (c)

Fig. 13 The component fabricated based on the R-LOM and the NUP paths: (a) the overall view, (b) the cross-sectional profile, (c) layer surfaces

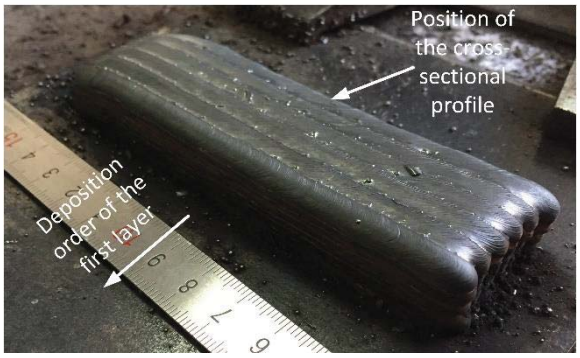

(a)

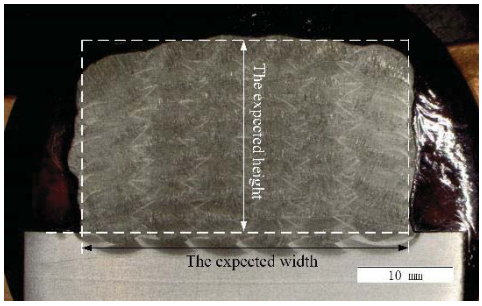

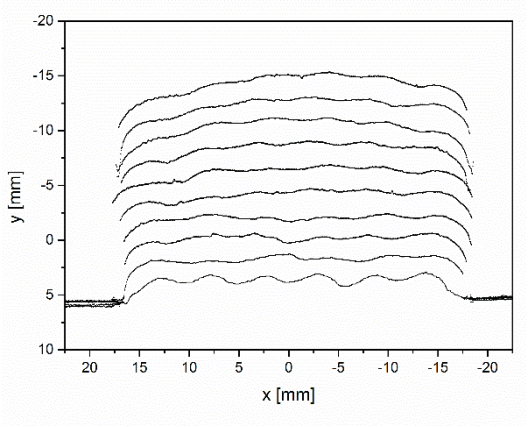

(b) (c)

Fig. 14 The component fabricated based on the R-LOM and the IRUP paths: (a) the overall view, (b) the cross-sectional profile, (c) layer surfaces

the dash lines) better than the components fabricated with the T-LOM. A quantitative evaluation of the four components is given below.

A comparison between the average widths of the layers with regard to the four fabricated components (2 with R-LOM and 2 with T-LOM) is presented in Fig. 15. The width of a layer was considered as the average value of 5 measurements on the middle part of the component (expect the starting and ending sections of the arc). The results show that the widths of the components fabricated according to the T-LOM were much smaller than the designed value of the layer width. This also implies the drawback of the material shortage areas in the case of the T-LOM. In industrial applications, the narrowed width of the layers might need additional deposition process to be fixed, or might make the fabricated part scrapped. As a contrast, the widths of the component fabricated with the R-LOM were greater than the expected value. When the entire component had been fabricated, the redundant portions can be removed by an adequate machining process.

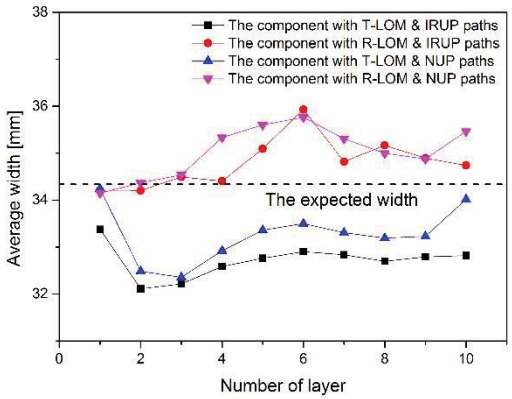

Fig. 15 Average widths of the layers of the fabricated four components

Moreover, the vertical distance between the substrate and the average height of the 10th layer of a component was considered as the height of the component. The same measurement principle was applied to measure the average heights of the four fabricated components. The results were shown in Table 2. In can be seen that the components fabricated with T-LOM were lower and narrower than the expected values. This is because that in the considered layer-overlapping model proposed in Figure 2, the expected cross-sectional profile of the component includes many material shortage areas. Therefore, the expected area is bigger than the deposited area with T-LOM in nature.

Table 2 The average height of the four fabricated components

Conditions	The average height (mm)
T-LOM & NUP paths	19.518
T-LOM & IRUP paths	20.138
R-LOM & NUP paths	19.814
R-LOM & IRUP paths	19.880

In addition, none of these four components met the expected value of height, which was 20.810 mm. The reason can be explained as follows: the geometric parameters of a single weld bead (e.g. width, height) deposited on the substrate were considered as a reference to design the manufacturing parameters of the whole component. It was one of our assumptions in the background research. However, the condition of heat dissipation of the single weld bead deposited on the substrate was rather different from the conditions of the rest beads of the component. The different heat dissipation conditions resulted in slight differences in terms of the geometric

parameters of the weld beads. That is, the weld beads in the lap layers tended to be lower and wider than the single weld bead deposited on the substrate. This is also one of the reasons why the layer widths of the component produced according to the R-LOM were greater than the expected value.

To support a quantitative evaluation of the layer surfaces, two parameters were defined: (i) flatness of the surface (FoS), which is used to evaluate if the surface of a layer is flat or not, and (ii) deviation from the expected height (DEH), which is used to evaluate how much the surface of a deposited layer deviates from the expected layer surface. Let us define μ as the average height of the surface of a deposited layer, which is calculated as follows:

$$\mu = \frac{1}{N}\sum_{i=1}^{N} H_i \tag{11}$$

where: H_i is the height value of a point measured on the layer surface, and N indicates the number of measured points on the layer surface. With this, the FoS of a deposited layer can be calculated so as:

$$\mathrm{FoS} = \frac{1}{N}\sum_{i=1}^{N} (H_i - \mu)^2 \tag{12}$$

If H_e is defined as the expected height of a deposited layer, then the DEH can be calculated so as:

$$DEH = \frac{1}{N}\sum_{i=1}^{N} (H_i - H_e)^2 \tag{13}$$

Based on the Equations (12) and (13), the layer surfaces of the fabricated components were evaluated. For each component, the cross-sectional profiles at 5 positions along the deposition direction without the starting and ending sections of arc were considered to calculate the average values. The results are shown in Fig. 16. It can be seen that the R-LOM enabled a steady increase of the layers and achieved a better surface flatness than the T-LOM when the component was deposited with NUP paths, whereas the R-LOM played a limited role with regard to the layer surface flatness when the IRUP paths were applied. This is because that the alternative deposition of first bead and last bead at the edges alleviates the accumulation of material shortage areas

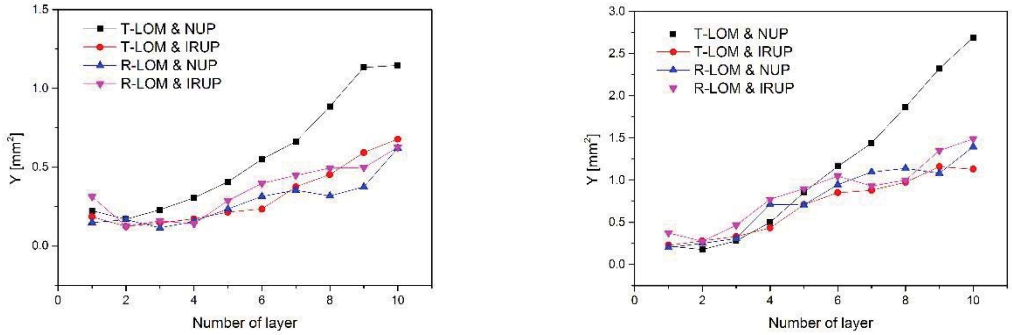

(a) (b)

Fig. 16 Evaluation results of the layer surfaces of the components: (a) FOS of the layers, (b) DEH of the layers

caused by the first bead, which enables a steady increase of the layers. It is also the reason why the components fabricated with the IRUP paths were narrower and higher than the components fabricated with the NUP paths.

5. Conclusions

In this paper, the layers-overlapping process of a cuboid component is in the focus. The layers-overlapping process was analyzed from a mathematical point of view and the limitations of the T-LOM were identified. According to the proposed model, it has been found that the average height of a layer's edge is smaller than the average height of the layer's main body, which causes generation of material shortage areas at the edges of the layers. It is validated that the material shortage areas reduce the width of the fabricated components. In addition, when multiple layers are overlapped, accumulation of the material shortage areas reduces the height of the first bead of the component when NUP paths were applied for deposition.

To deal with this problem, a LOS was proposed. The LOS suggests that the deposition amount of the first bead and the last bead of the lap layers should be increased. In addition, the deposition positions of the first bead and the last bead of the lap layers should be moved towards the edge of the layer with an offset distance. Validation experiments have been conducted considering two path strategies, namely the NUP paths and the IRUP paths. Based on the experimental observations, the R-LOM in combination with the proposed LOS covered the material shortage areas of the lap layers. The advantage of the R-LOM is that it enables the cuboid components to

achieve the expected width. In addition, for components deposited with NUP paths, the R-LOM eliminates the effect of accumulation of material shortage areas on the first bead and increases the surface flatness. The NUP paths is a basis of the curved unidirectional parallel (CUP) paths. Both strategies are normally employed in the path-planning strategies of additive manufacturing for complex structures in the practice. Therefore, the proposed LOS is an important step towards near-net-shaping of MLMB components fabricated by WAAM.

In the design period for the manufacturing parameters, deformation of the component was neglected. In addition, it was assumed that all the weld beads in the fabricated component were considered as the same as the single weld bead deposited on the substrate. These two issues made the fabricated components lower than the expected CAD model. We concluded that the manufacturing parameters designed based on the single weld bead models deposited on a substrate are not accurate enough for near-net-shaping of MLMB components. However, it is hardly possible to develop an accurate single weld bead model in which all the conditions, e.g. positions of the beads in an MLMB component and different temperature fields, are taken into consideration. This is because that the models of the weld beads at different positions of a MLMB component are different. Therefore, this phenomenon implies the need for process control actions in order to further improve the geometric accuracy of the MLMB components fabricated by WAAM, which will be the topic of our follow-up research.

Acknowledgement

This work was supported by National Natural Science Foundation of China, No. 51575133.

References

1. Zhang Y, Chen Y, Li P, Male AT (2003) Weld deposition-based rapid prototyping: a preliminary study. Journal of Materials Processing Technology 135(2-3):347-357
2. Spencer JD, Dickens PM, Wykes CM (1998) Rapid prototyping of metal parts by three-dimensional welding. Proceedings of the Institution of Mechanical Engineers Part B Journal of Engineering Manufacture 212(3):175-182
3. Williams SW, Martina F, Addison AC, Ding J, Pardal G, Colegrove P (2016) Wire + Arc Additive Manufacturing. Materials Science and Technology 32(7):641-647
4. Zhang Y, Li P, Chen Y, Male AT (2002) Automated system for welding-based rapid prototyping. Mechatronics 12(1):37-53
5. Ding D, Pan Z, Cuiuri D, Li H (2015) Wire-feed additive manufacturing of metal components:

technologies, developments and future interests. The International Journal of Advanced Manufacturing Technology 81(1-4):465-481

6. Xiong J, Zhang G, Hu J, Li Y (2013) Forecasting process parameters for GMAW-based rapid manufacturing using closed-loop iteration based on neural network. The International Journal of Advanced Manufacturing Technology 69(1):743-751
7. Kwak YM, Doumanidis CC (2002) Geometry Regulation of Material Deposition in Near-Net Shape Manufacturing by Thermally Scanned Welding. Journal of Manufacturing Processes 4(1):28-41
8. Xiong J, Zhang G, Qiu Z, Li Y (2013) Vision-sensing and bead width control of a single-bead multi-layer part: material and energy savings in GMAW-based rapid manufacturing. Journal of Cleaner Production 41:82-88
9. Xiong J, Zhang G (2014) Adaptive control of deposited height in GMAW-based layer additive manufacturing. Journal of Materials Processing Technology 214(4):962-968
10. Song YA, Park S, Chae SW (2005) 3D welding and milling: part II—optimization of the 3D welding process using an experimental design approach. International Journal of Machine Tools and Manufacture 45(9):1063-1069
11. Karunakaran KP, Suryakumar S, Pushpa V, Akula S (2010) Low cost integration of additive and subtractive processes for hybrid layered manufacturing. Robotics and Computer-Integrated Manufacturing 26(5):490-499
12. Aiyiti W, Zhao W, Lu B, Tang Y (2006) Investigation of the overlapping parameters of MPAW-based rapid prototyping. Rapid Prototyping Journal 12(3):165-172
13. Cao Y, Zhu S, Liang X, Wang W (2011) Overlapping model of beads and curve fitting of bead section for rapid manufacturing by robotic MAG welding process. Robotics and Computer-Integrated Manufacturing 27(3):641-645
14. Suryakumar S, Karunakaran KP, Bernard A, Chandrasekhar U, Raghavender N, Sharma D (2011) Weld bead modeling and process optimization in Hybrid Layered Manufacturing. Comput Aided Design 43(4):331-344
15. Ding D, Pan Z, Cuiuri D, Li H (2015) A multi-bead overlapping model for robotic wire and arc additive manufacturing (WAAM). Robotics and Computer-Integrated Manufacturing 31:101-110
16. Li Y, Sun Y, Han Q, Zhang G, Horváth I (2017) Enhanced beads overlapping model for wire and arc additive manufacturing of multi-layer multi-bead metallic parts. Journal of Materials Processing Technology 252: 838-848
17. Xu F, Lv Y, Liu Y, Shu F, He P, Xu B (2013) Microstructural Evolution and Mechanical Properties of Inconel 625 Alloy during Pulsed Plasma Arc Deposition Process. Journal of Materials Science & Technology 29 (5):480-488

Figure 1

Click here to download Figure Figure 1.jpg

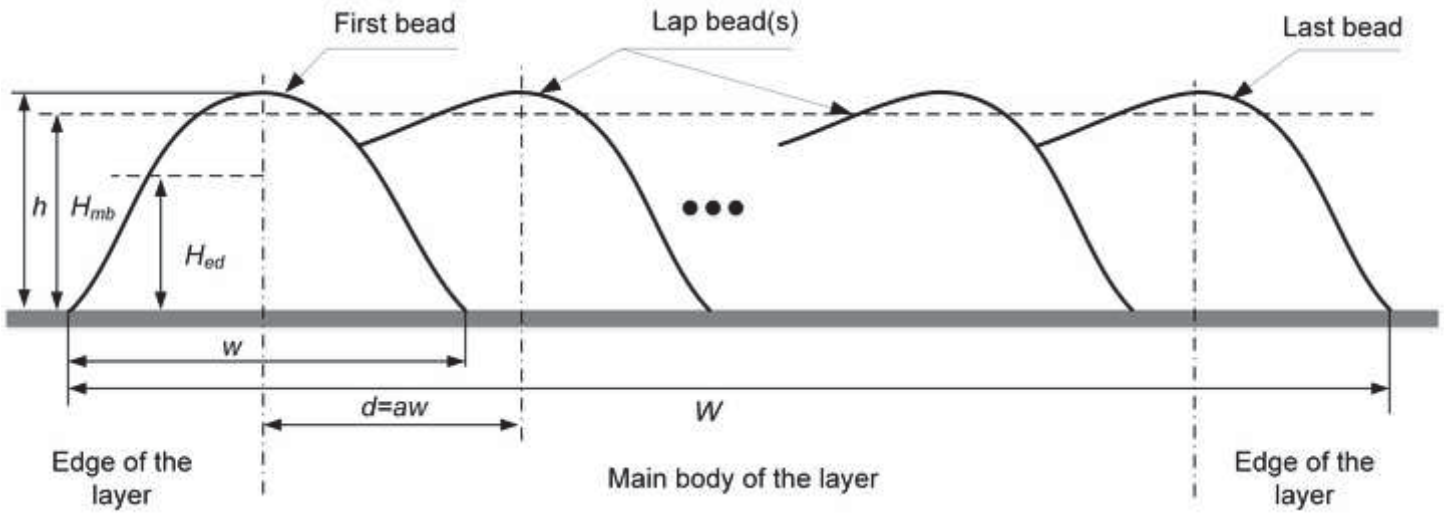

Figure 2

Click here to download Figure Figure 2.jpg

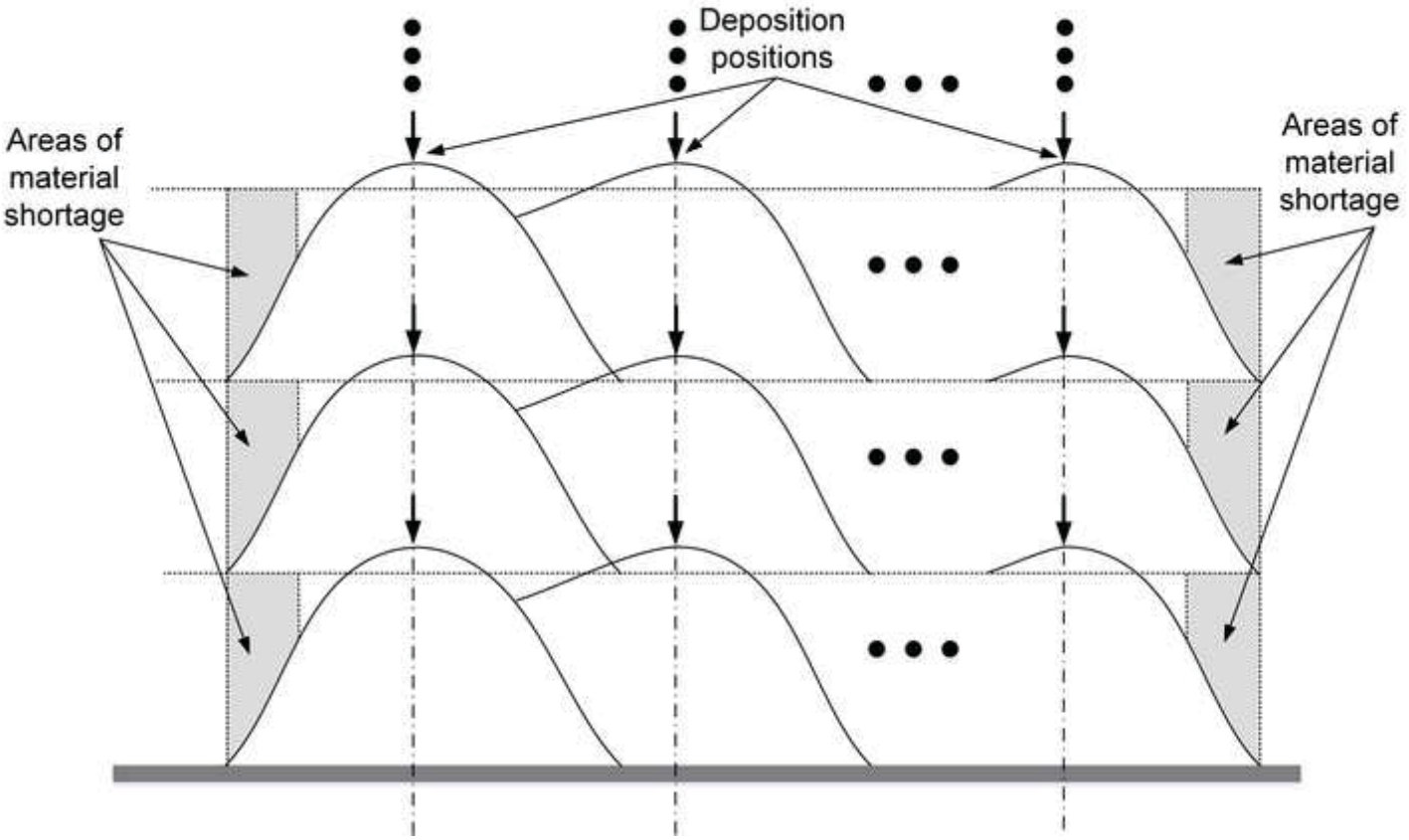

Figure 3

Click here to download Figure Figure 3.jpg

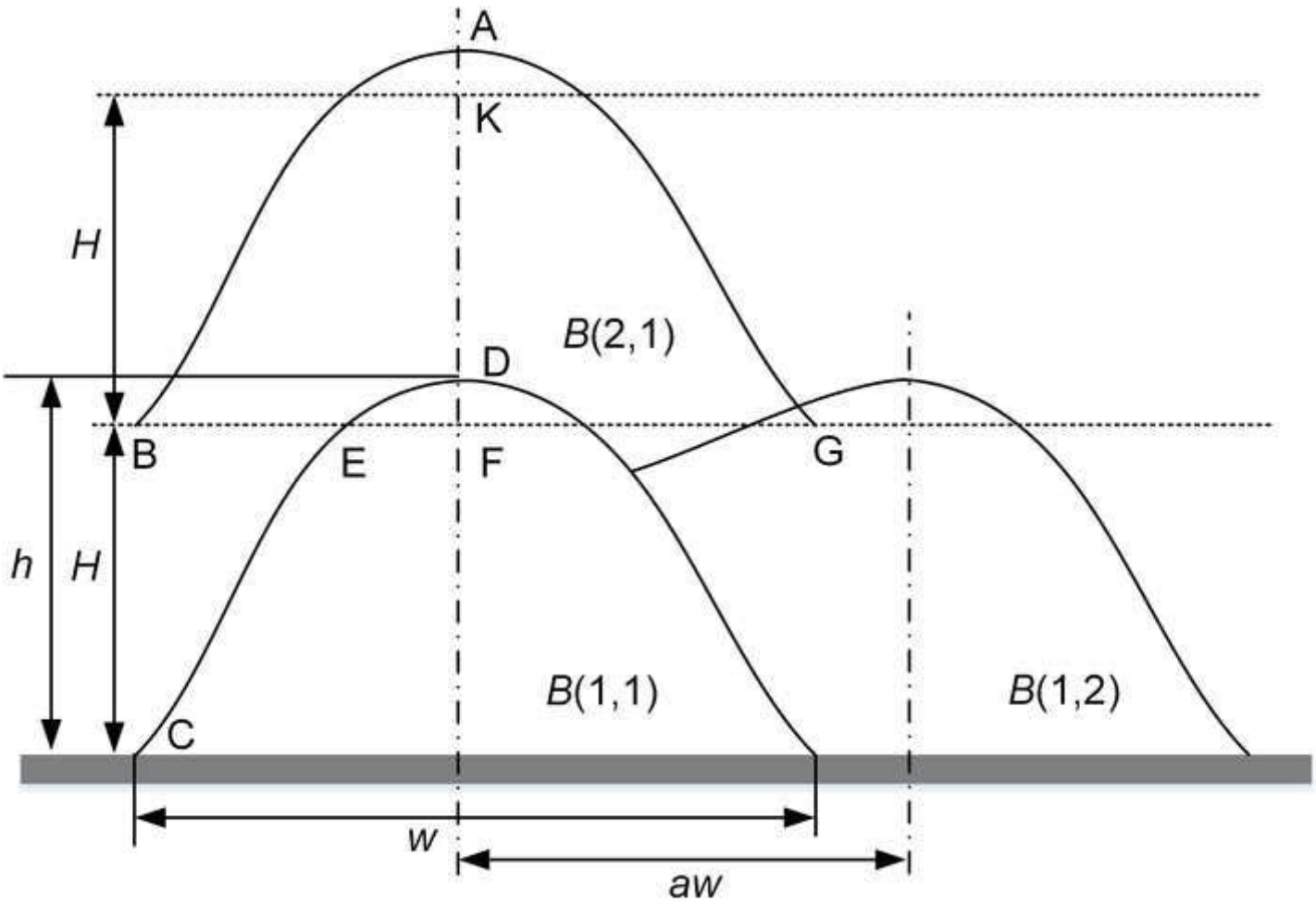

Figure 4

Click here to download Figure Figure 4.jpg

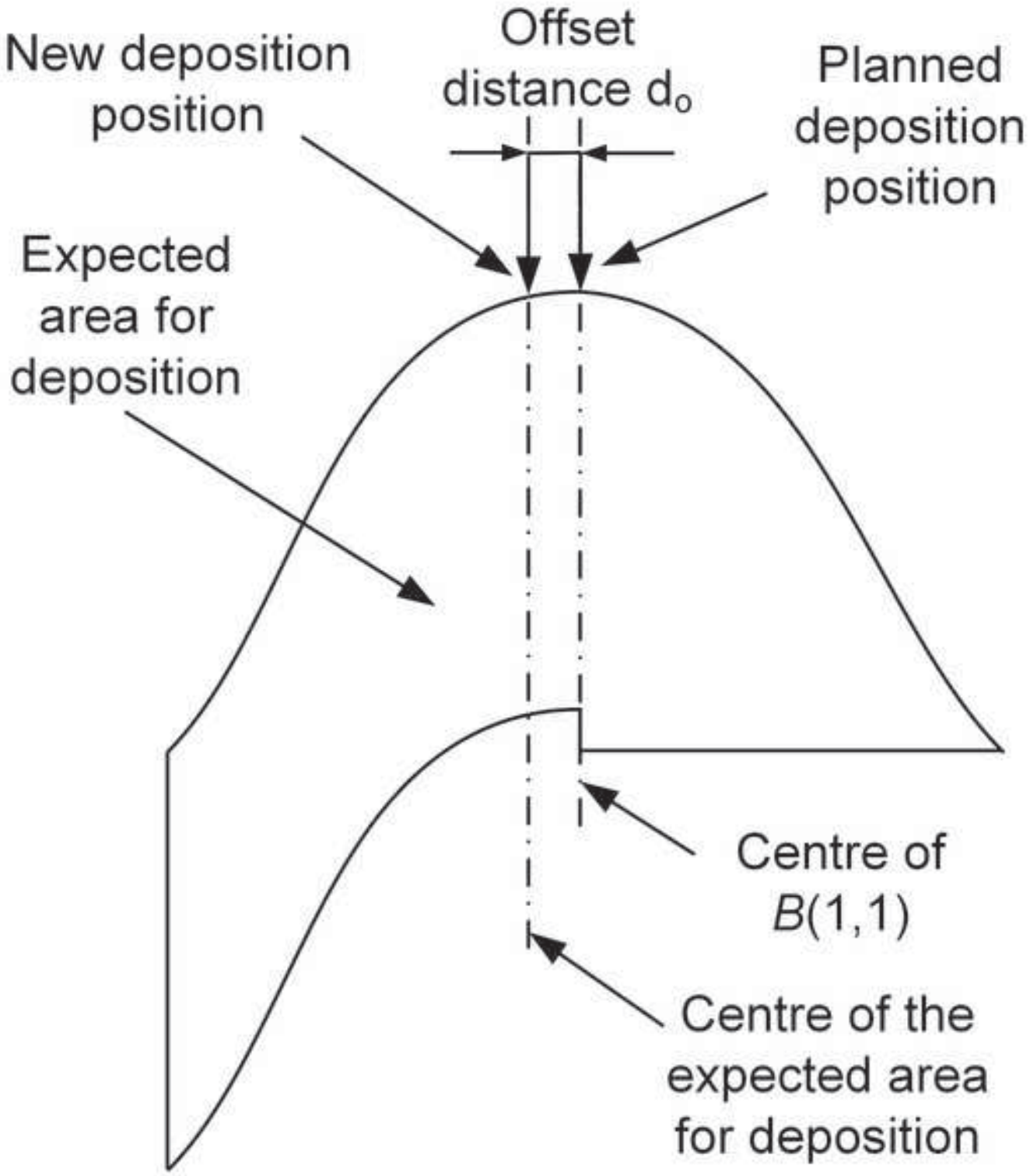

Figure 5

Click here to download Figure Figure 5.jpg

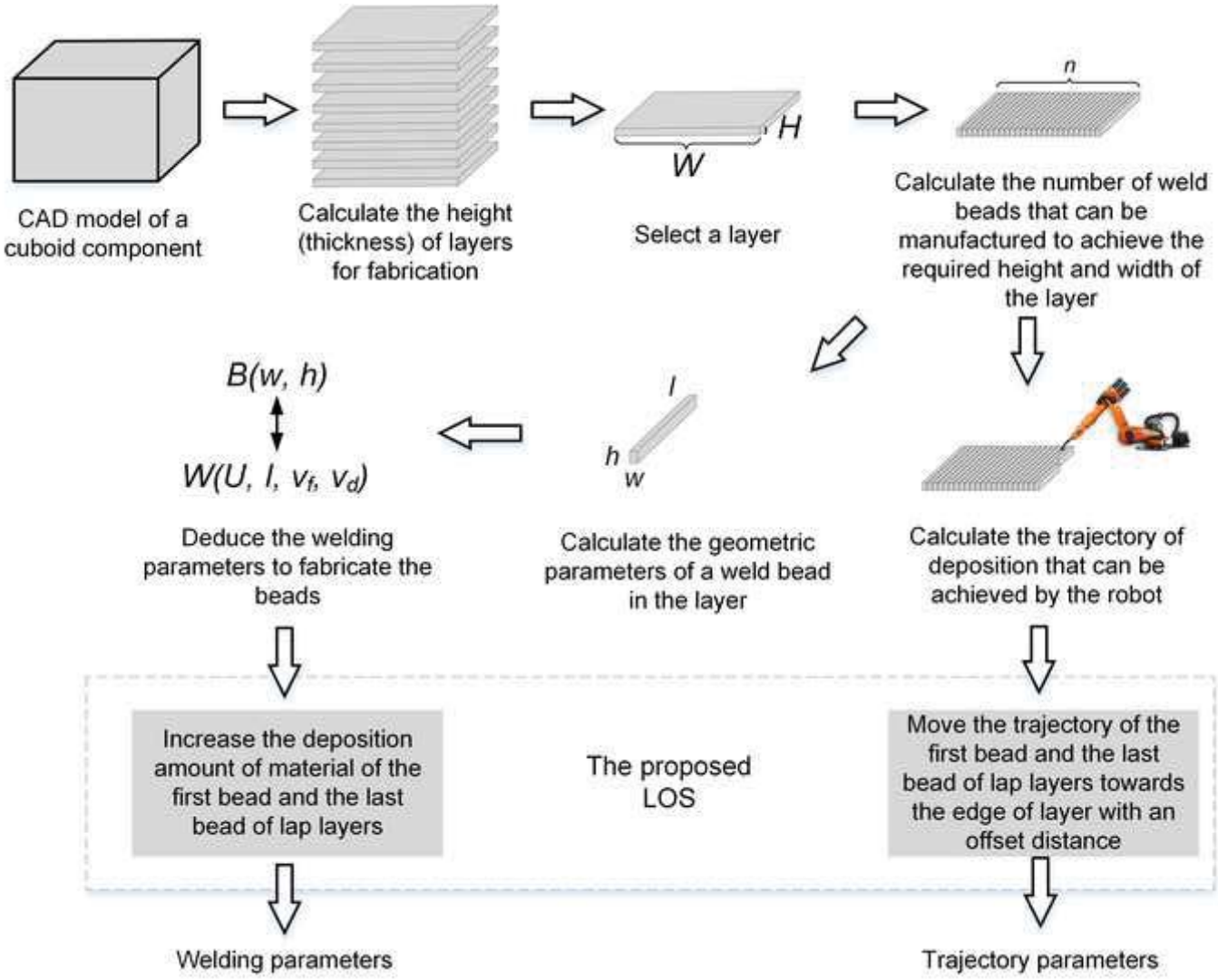

Figure 6

Click here to download Figure Figure 6.tif

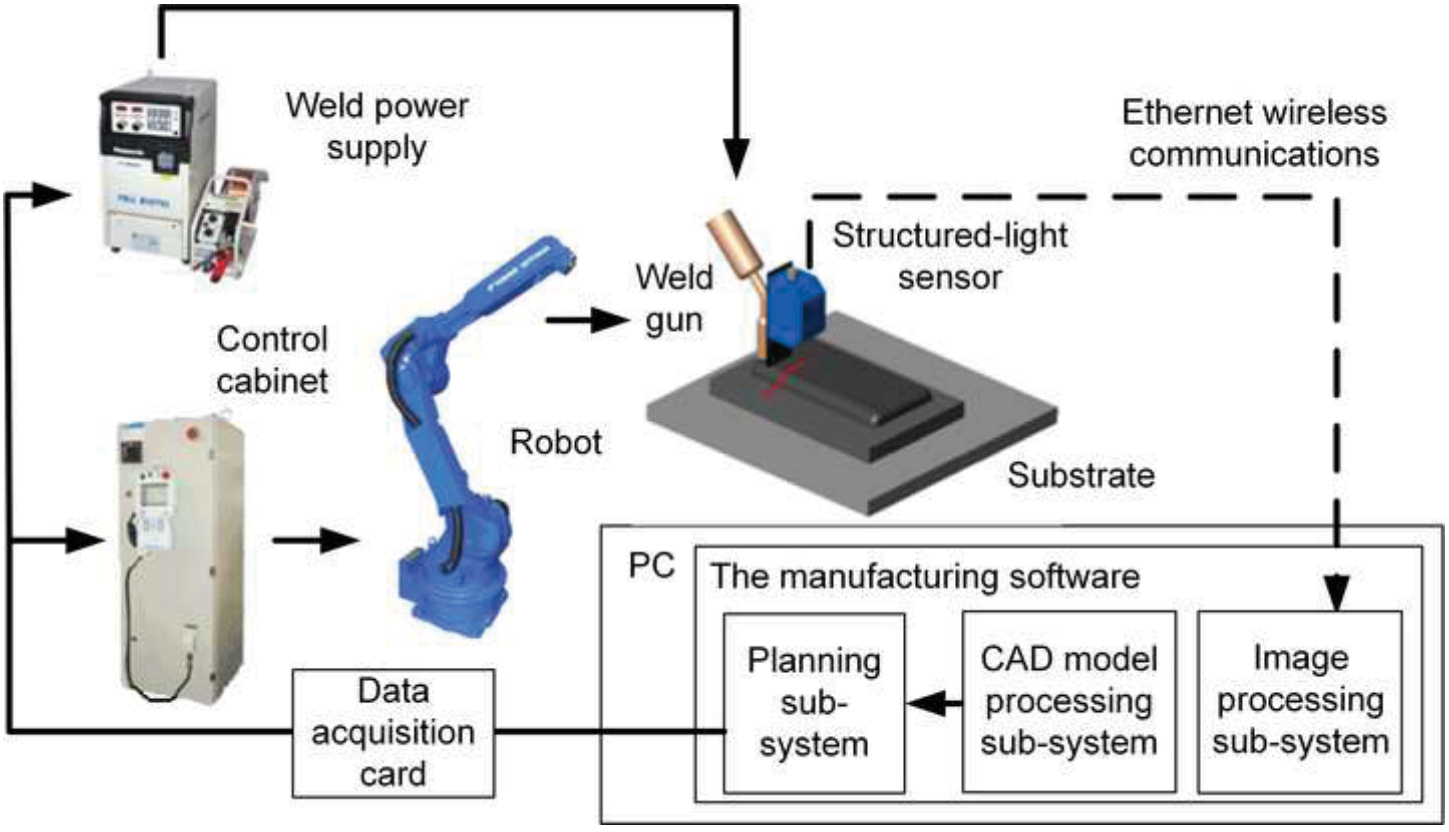

Figure 7a

Click here to download Figure Figure 7a.jpg

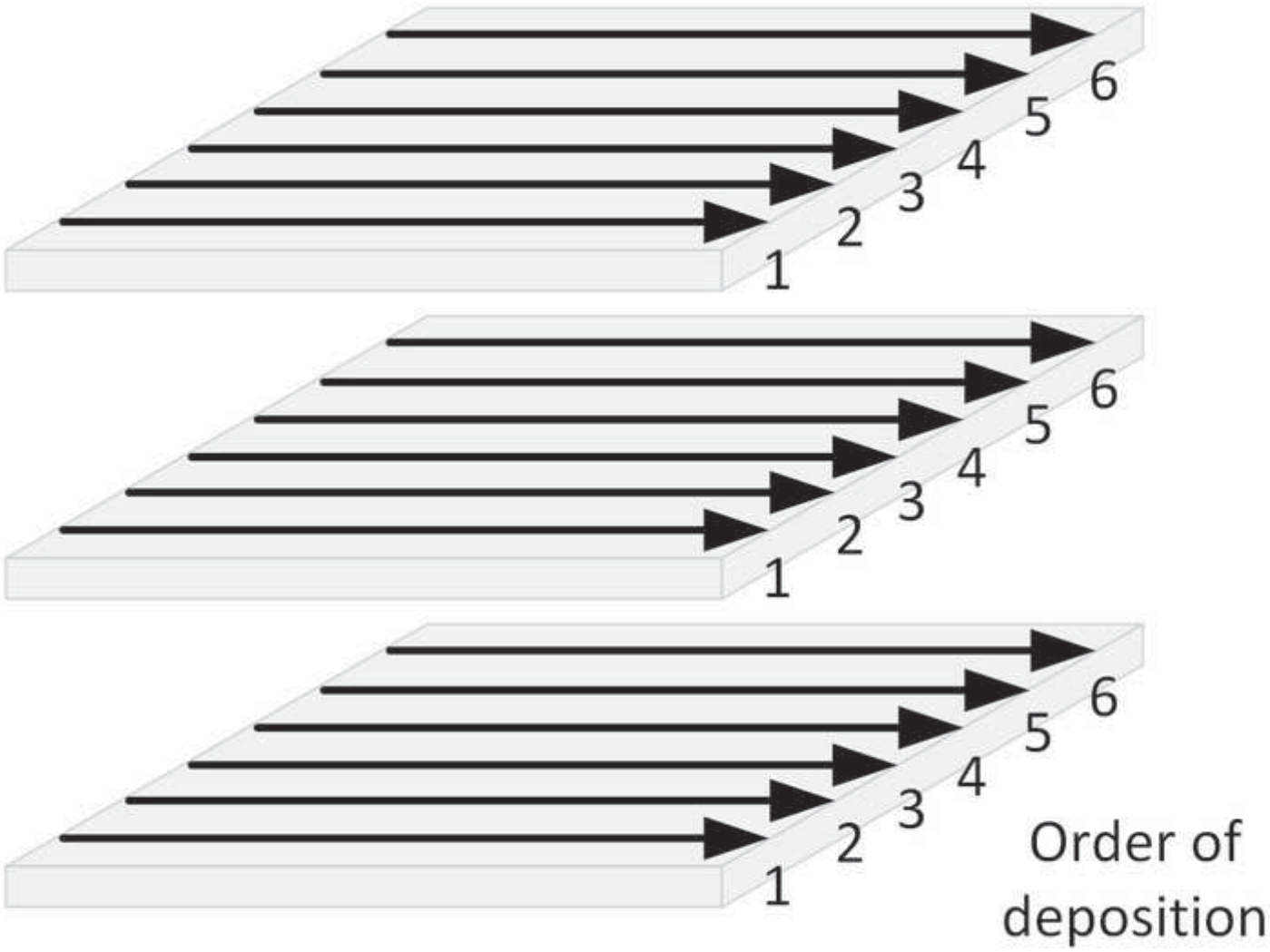

Figure 7b

Click here to download Figure Figure 7b.jpg

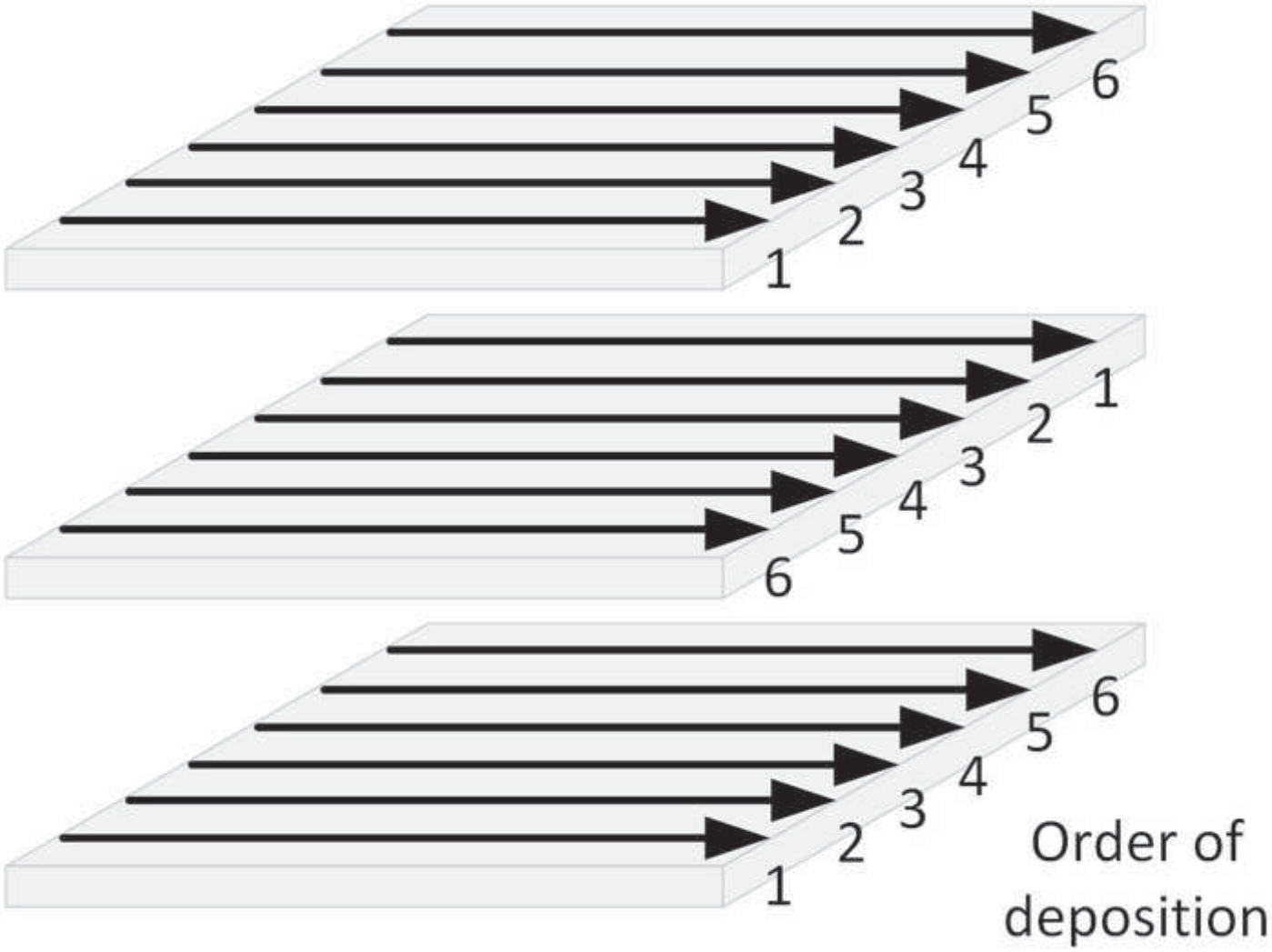

Figure 8a

Click here to download Figure Figure 8a.jpg

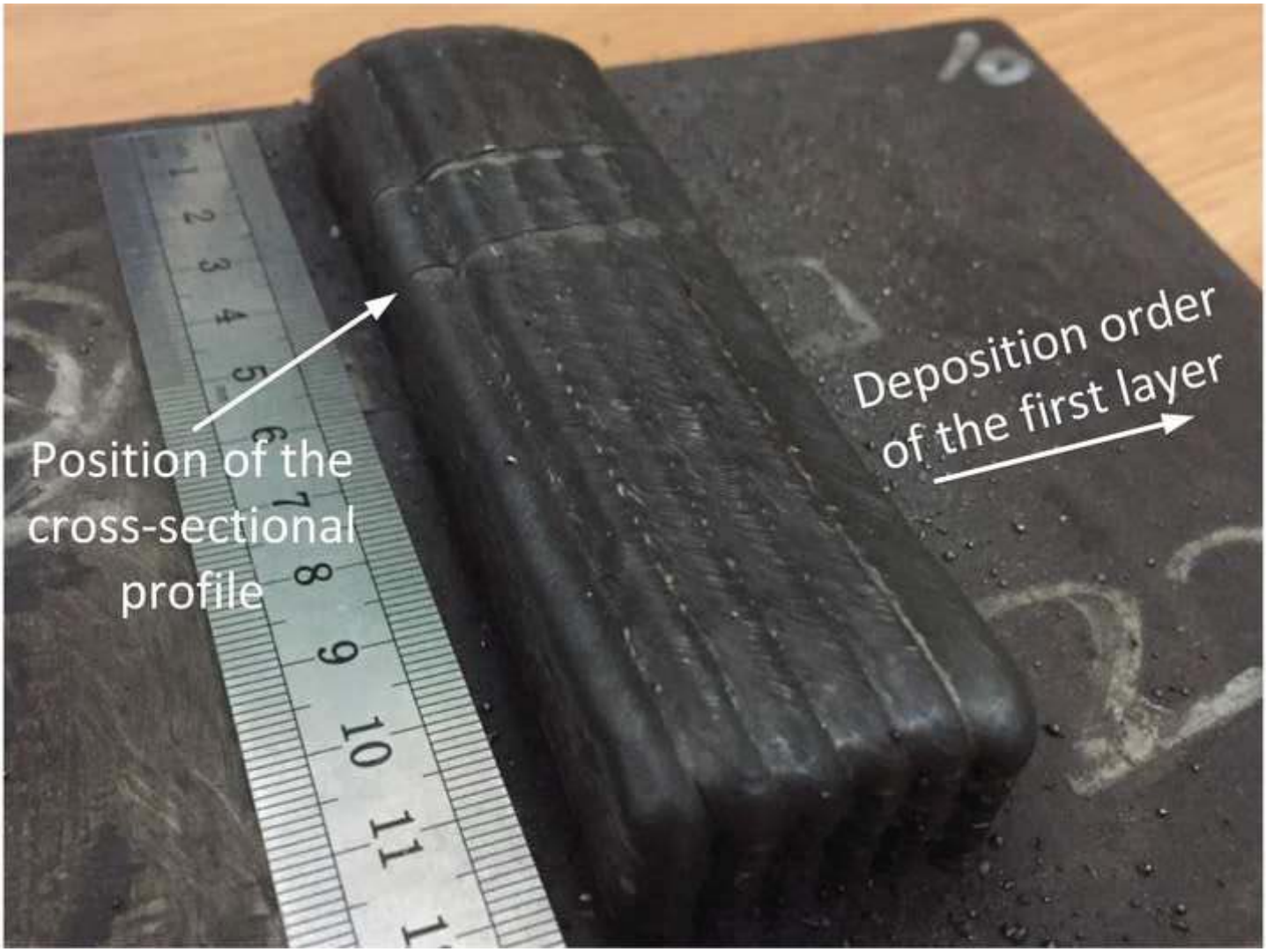

Figure 8b

Click here to download Figure Figure 8b.jpg

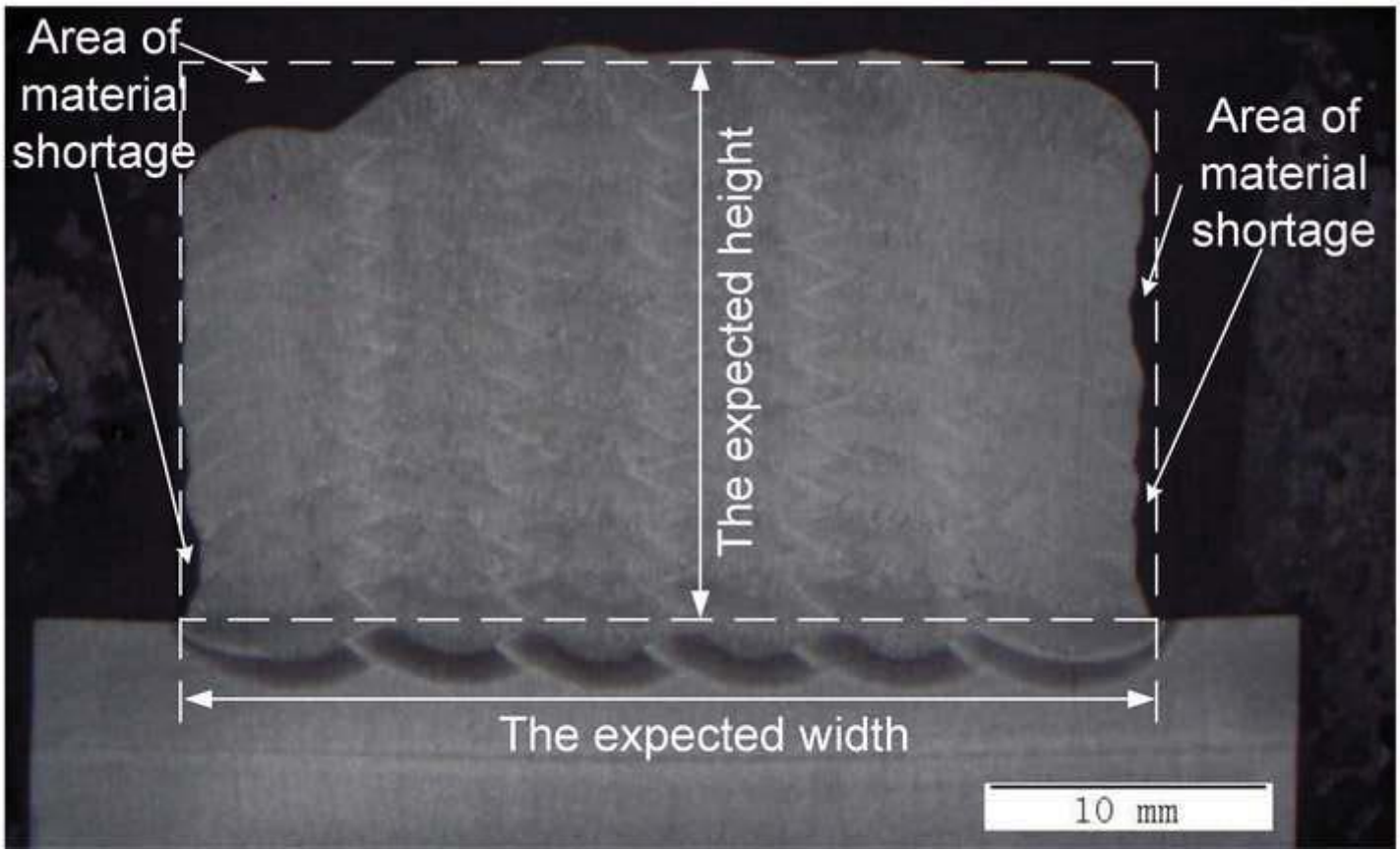

Figure 8c

Click here to download Figure Figure 8c.tif

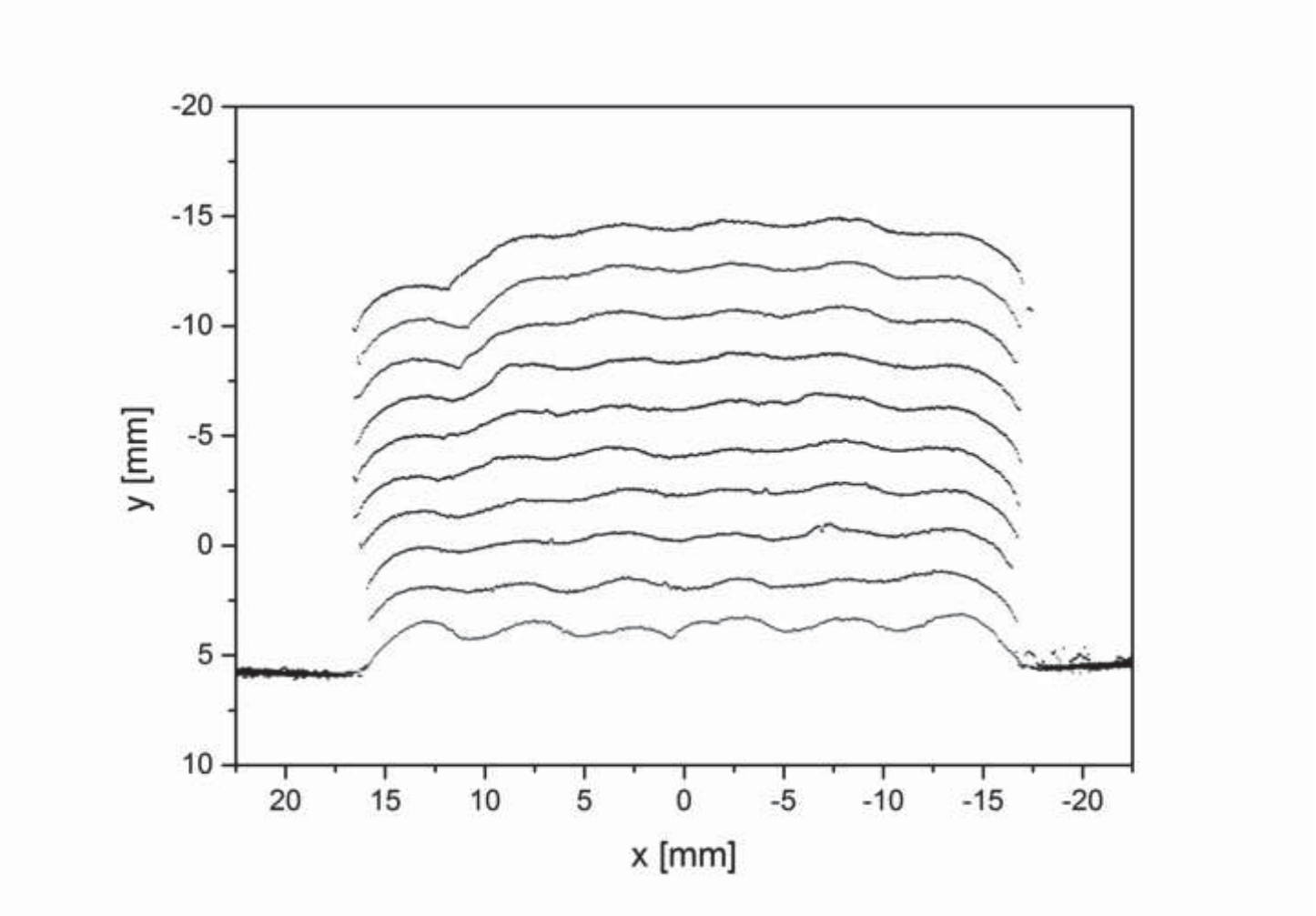

Figure 9a

Click here to download Figure Figure 9a.jpg

Figure 9b

Click here to download Figure Figure 9b.jpg

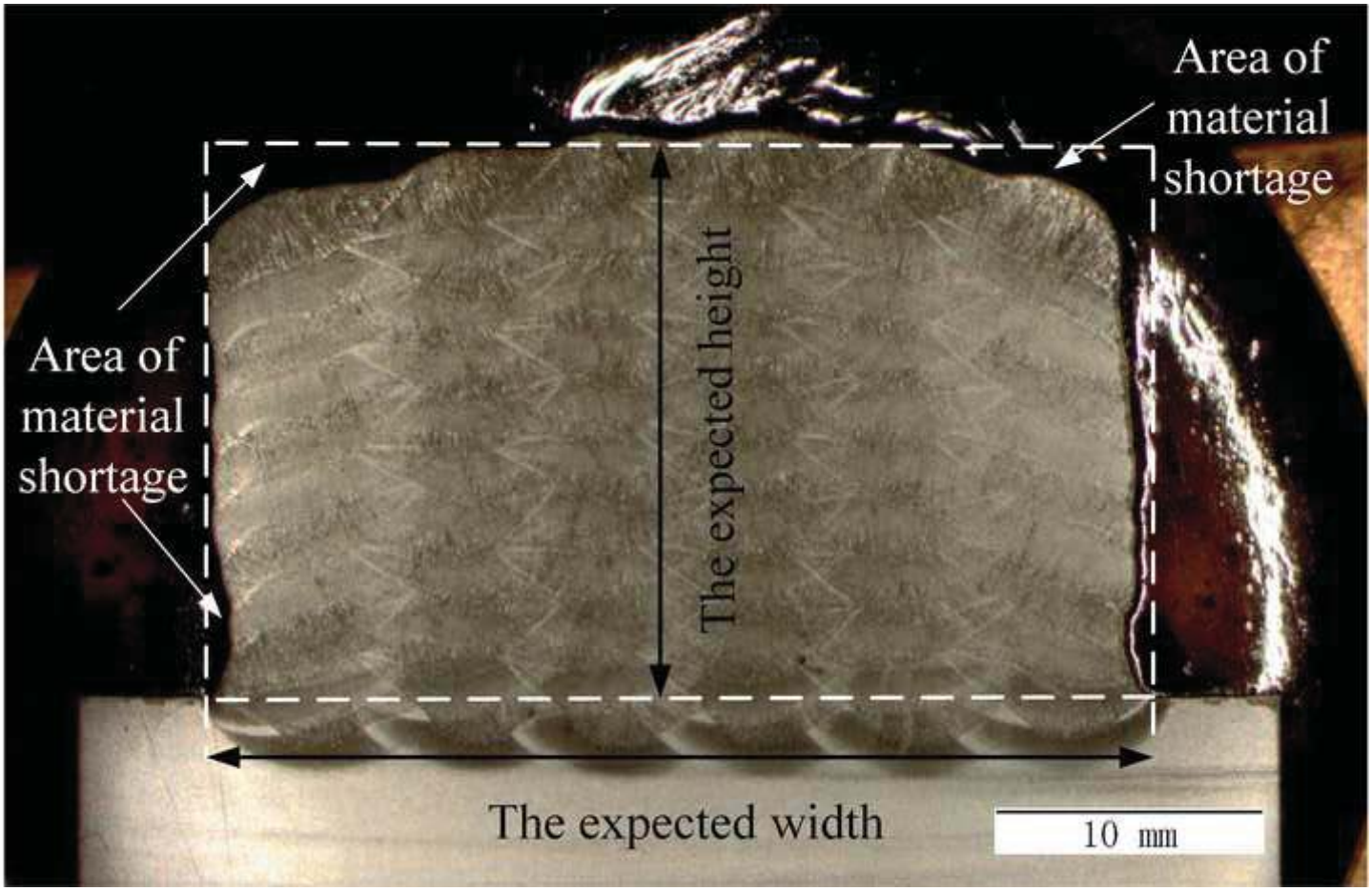

Figure 9c

Click here to download Figure Figure 9c.tif

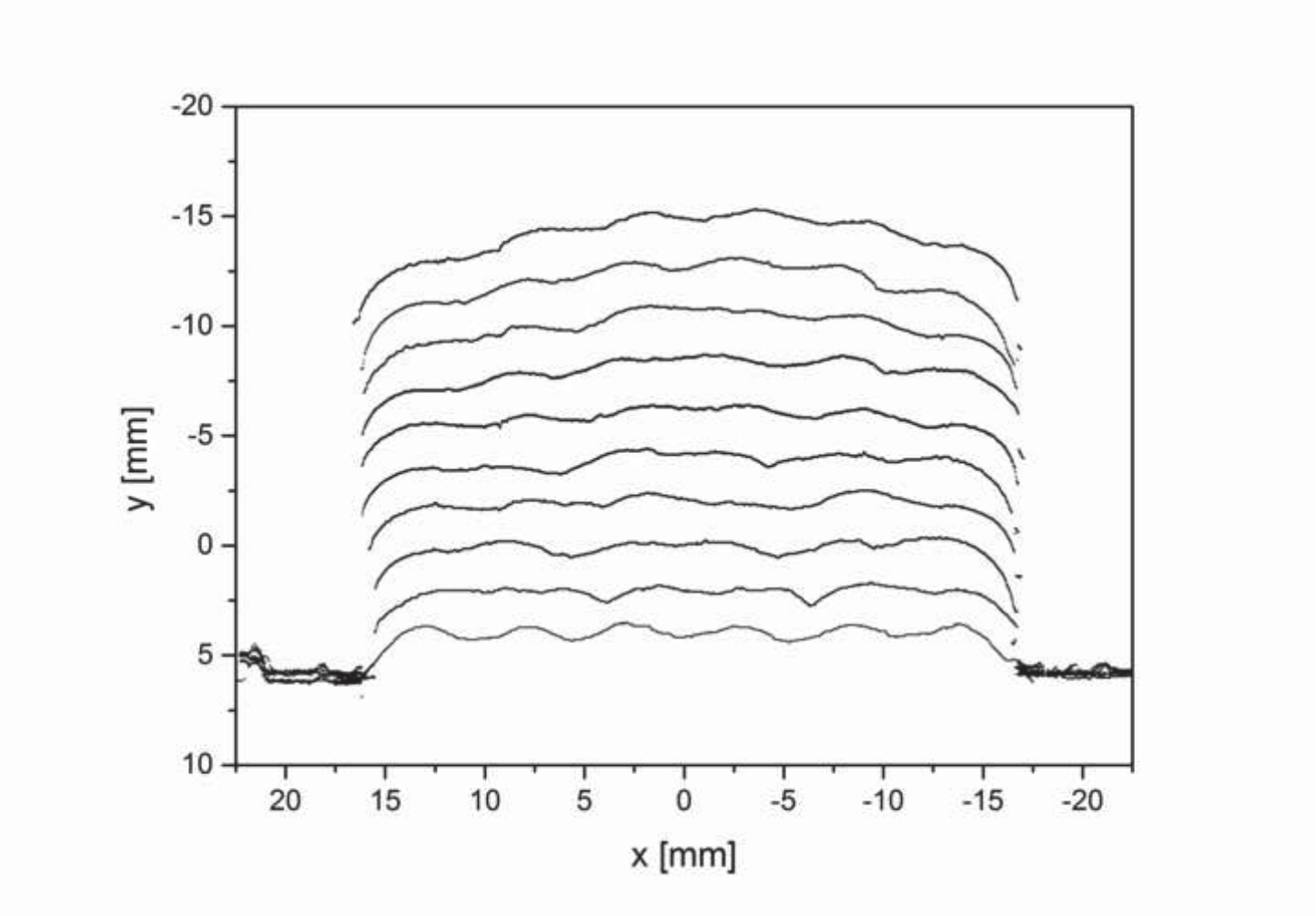

Figure 10a

Click here to download Figure Figure 10a.tif

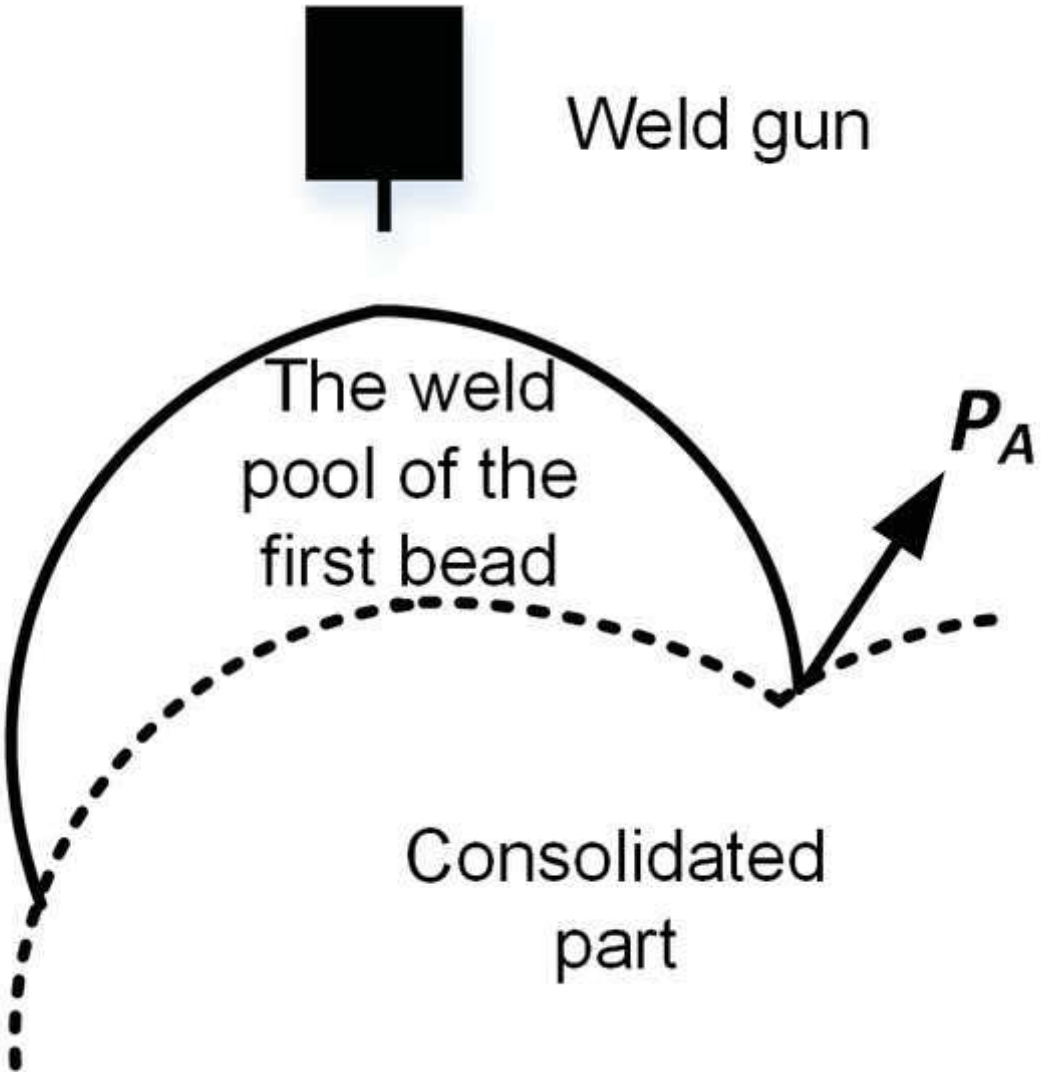

Figure 10b

Click here to download Figure Figure 10b.tif

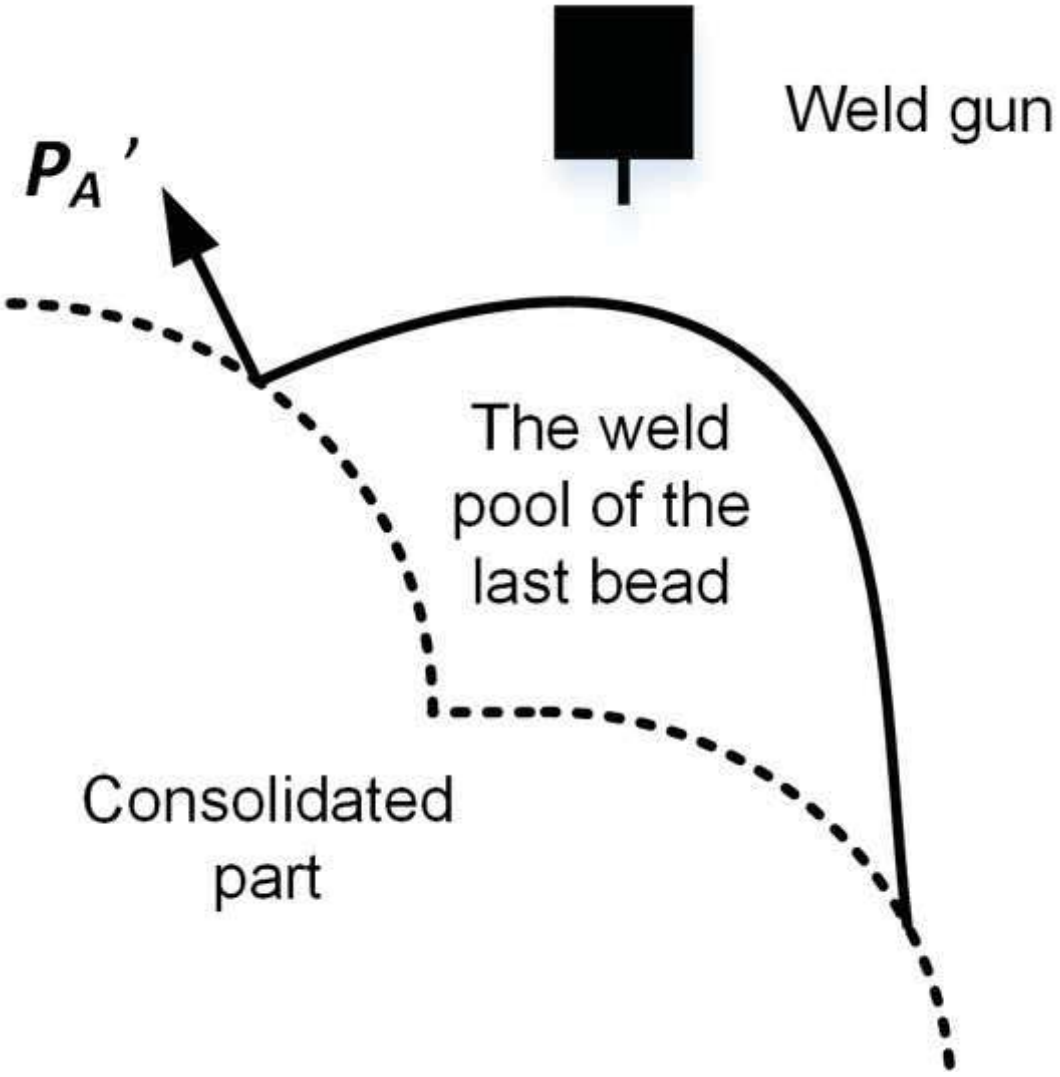

Figure 11a

Click here to download Figure Figure 11a.tif

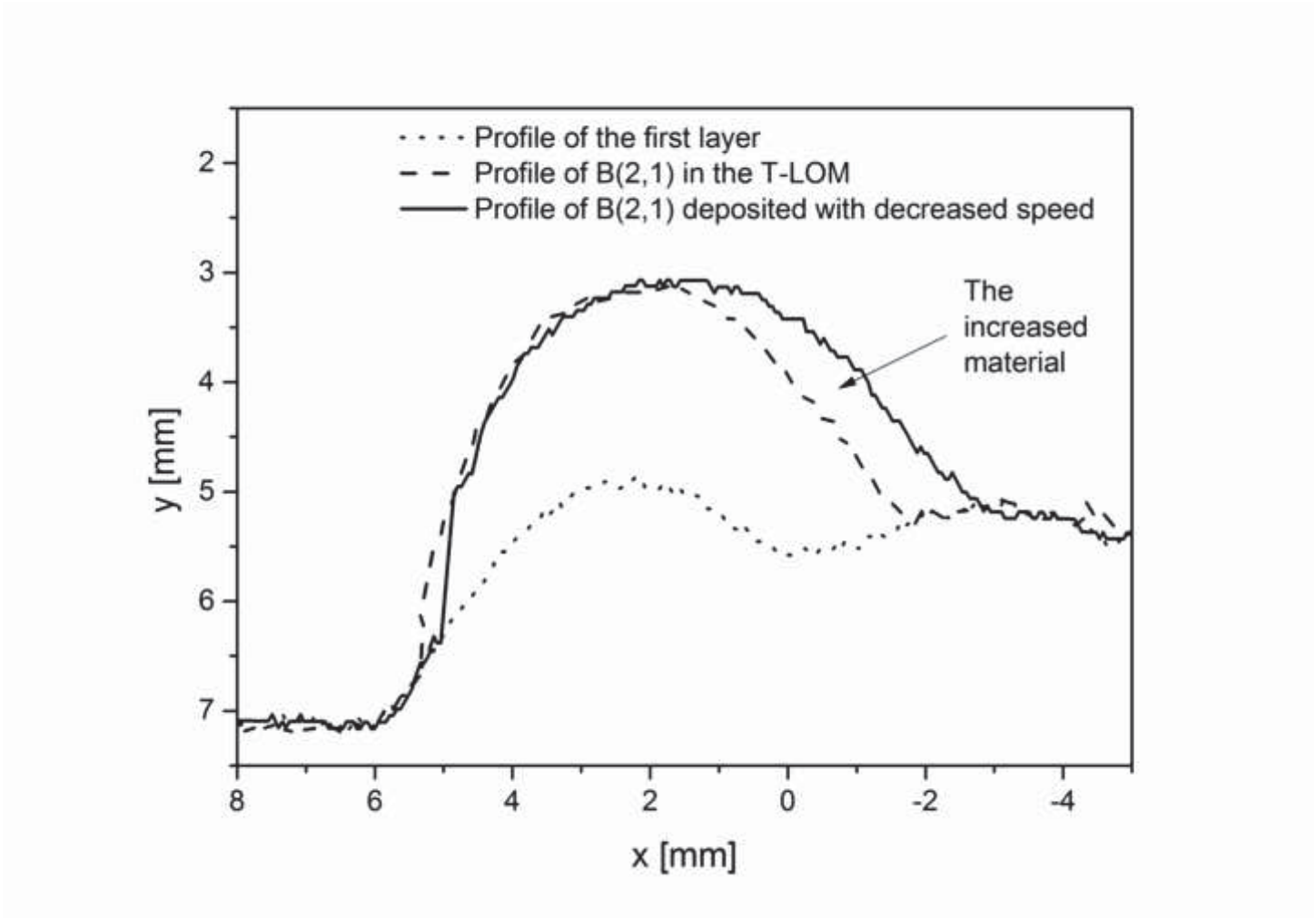

Figure 11b

Click here to download Figure Figure 11b.tif

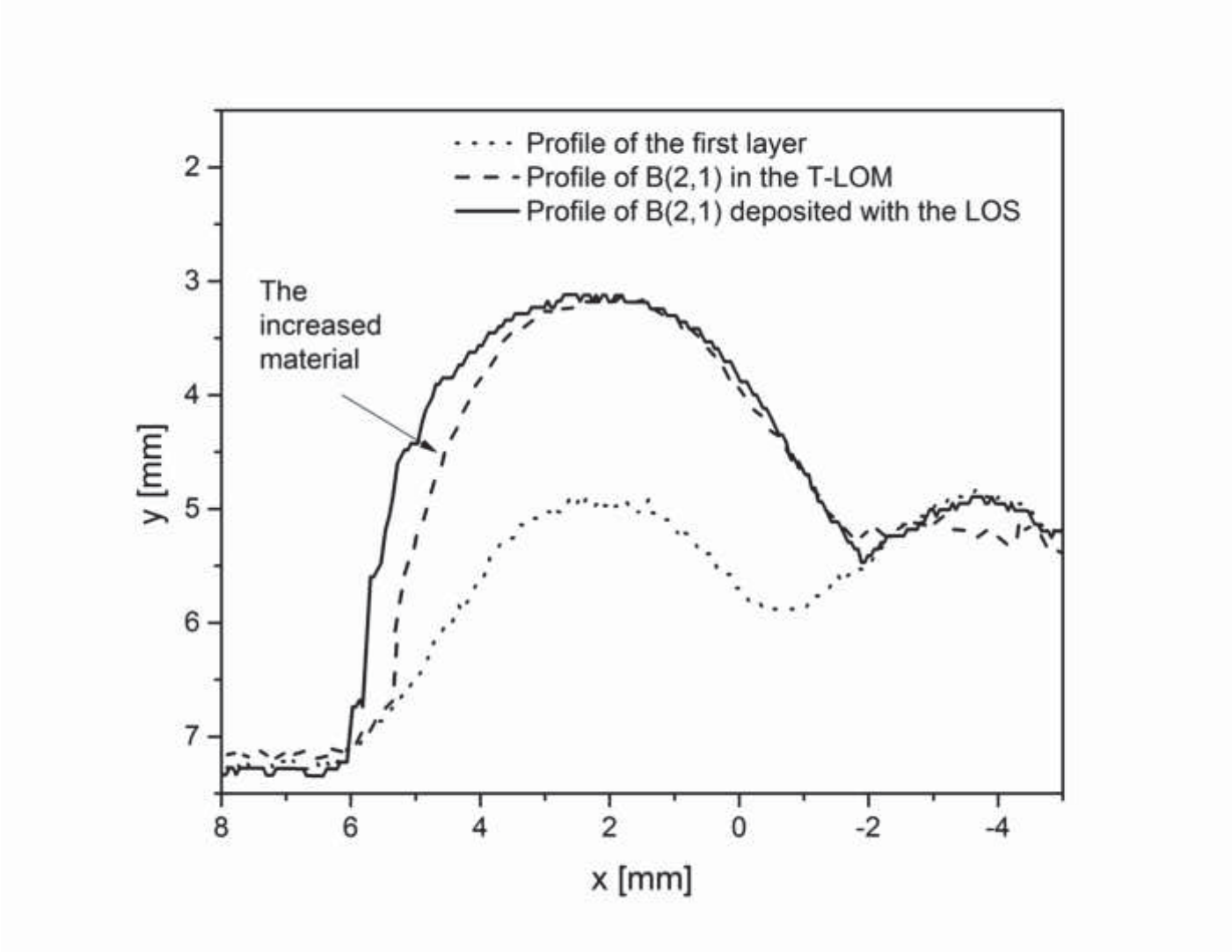

Figure 12a

Click here to download Figure Figure 12a.tif

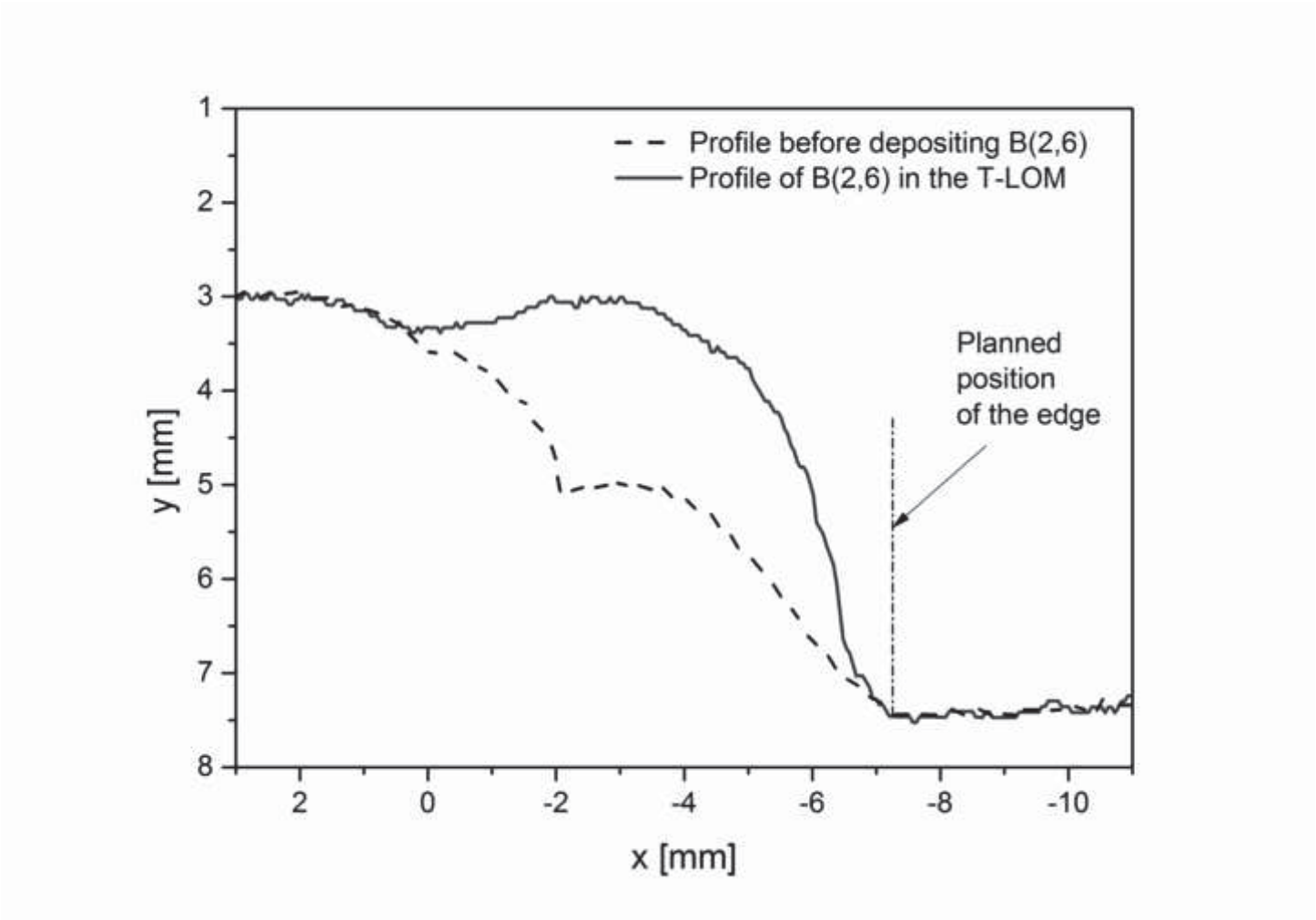

Figure 12b

Click here to download Figure Figure 12b.tif

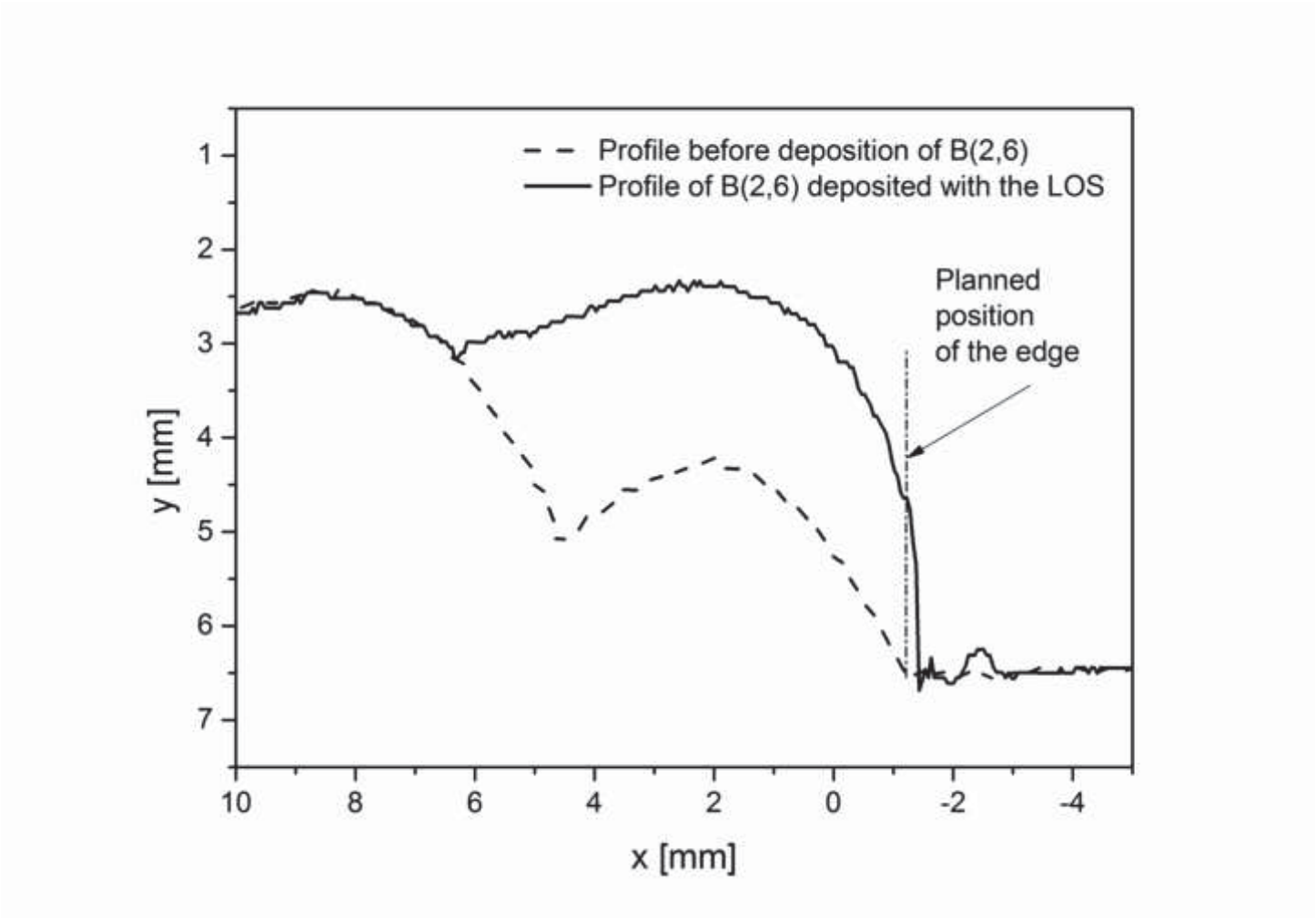

Figure 13a

Click here to download Figure Figure 13a.jpg

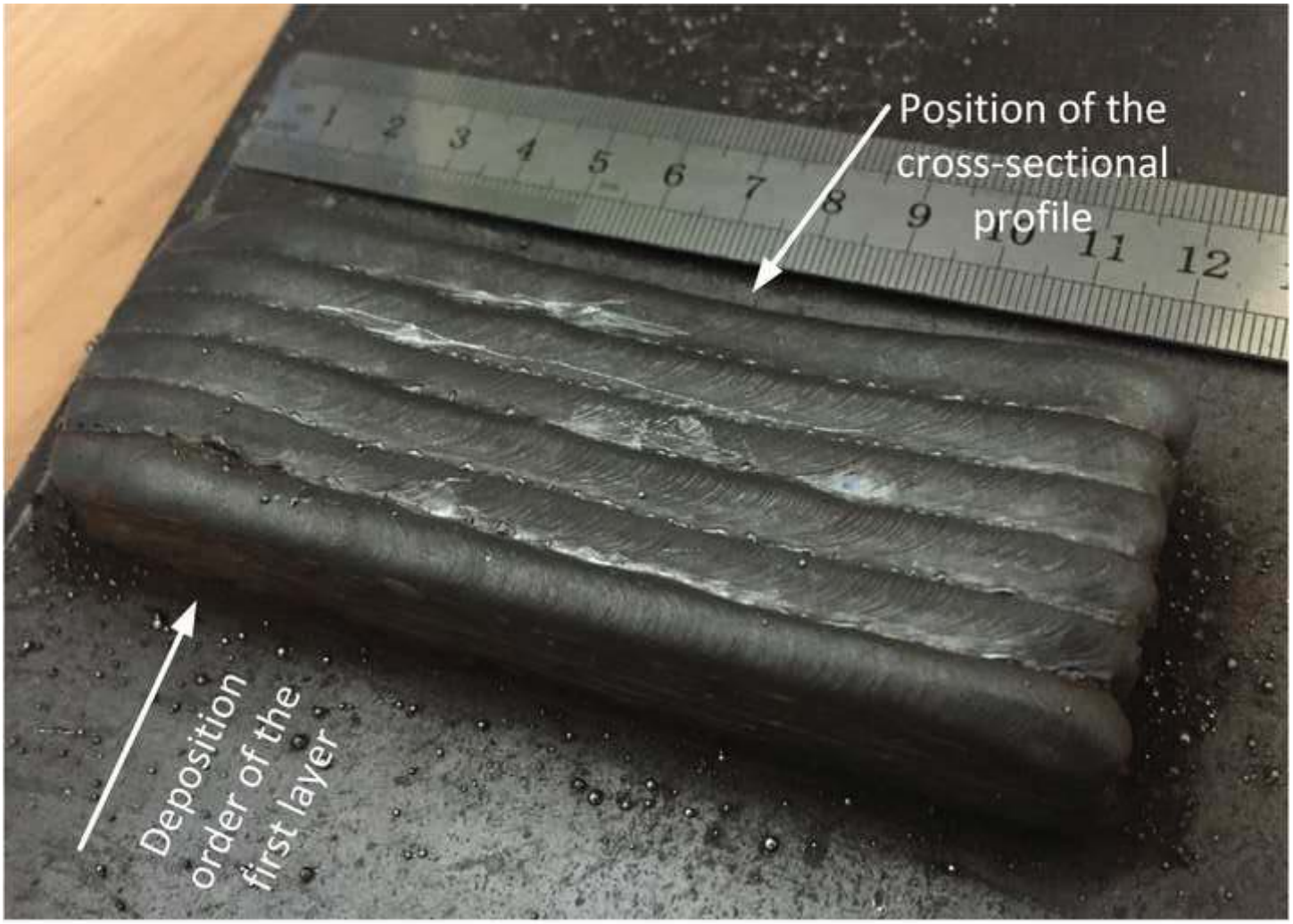

Figure 13b

Click here to download Figure Figure 13b.jpg

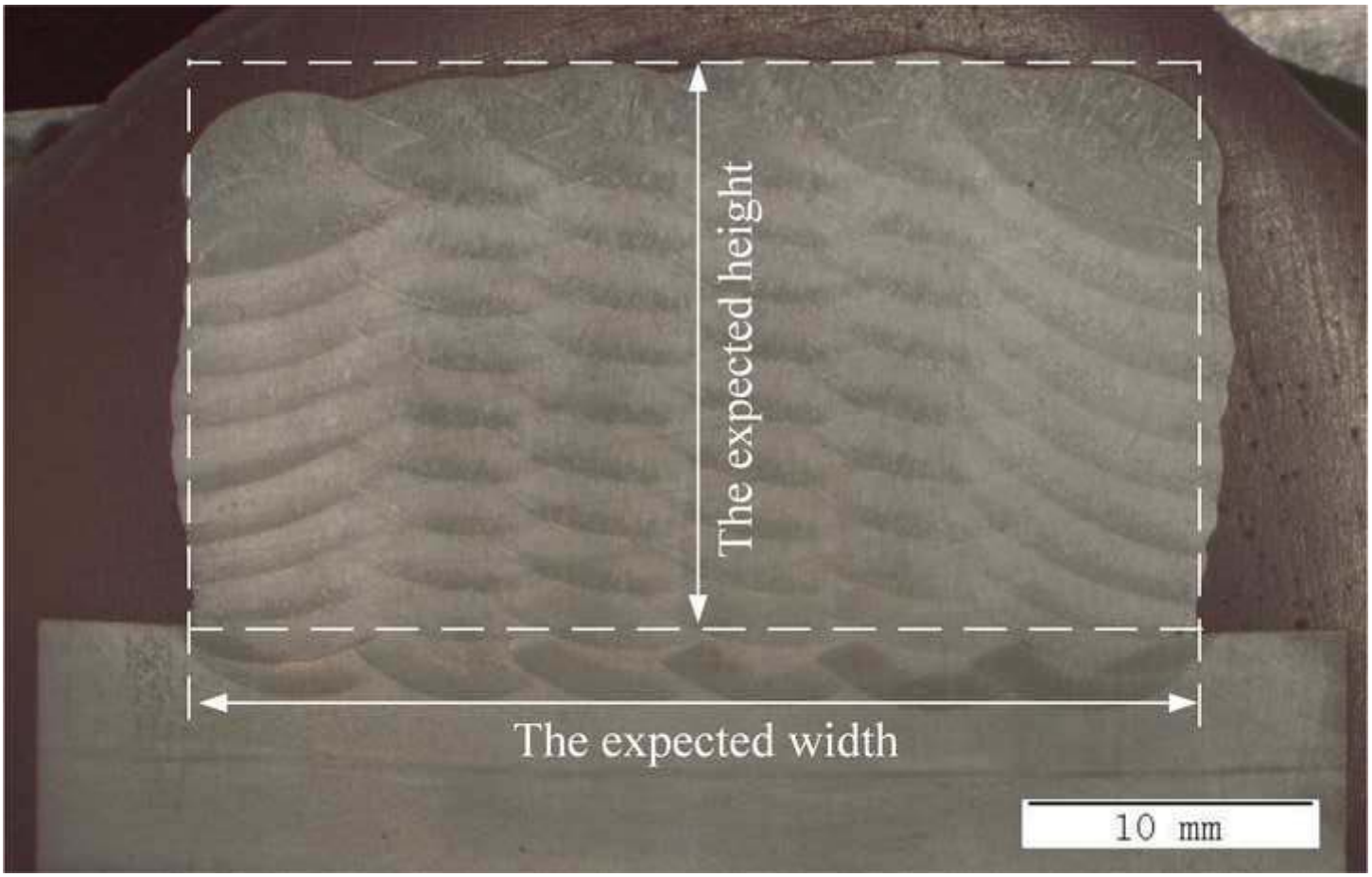

Figure 13c

Click here to download Figure Figure 13c.tif

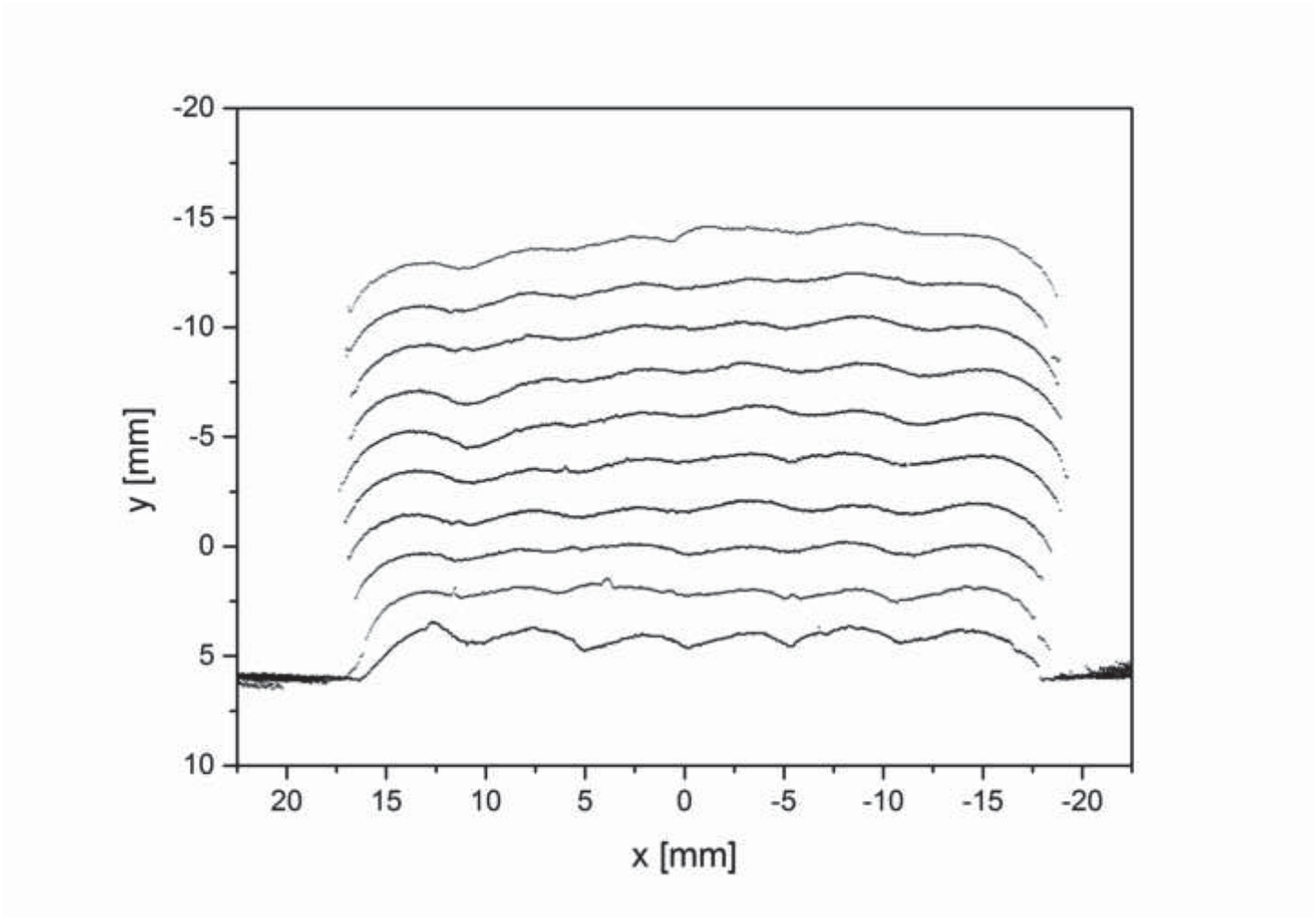

Figure 14a

Click here to download Figure Figure 14a.jpg

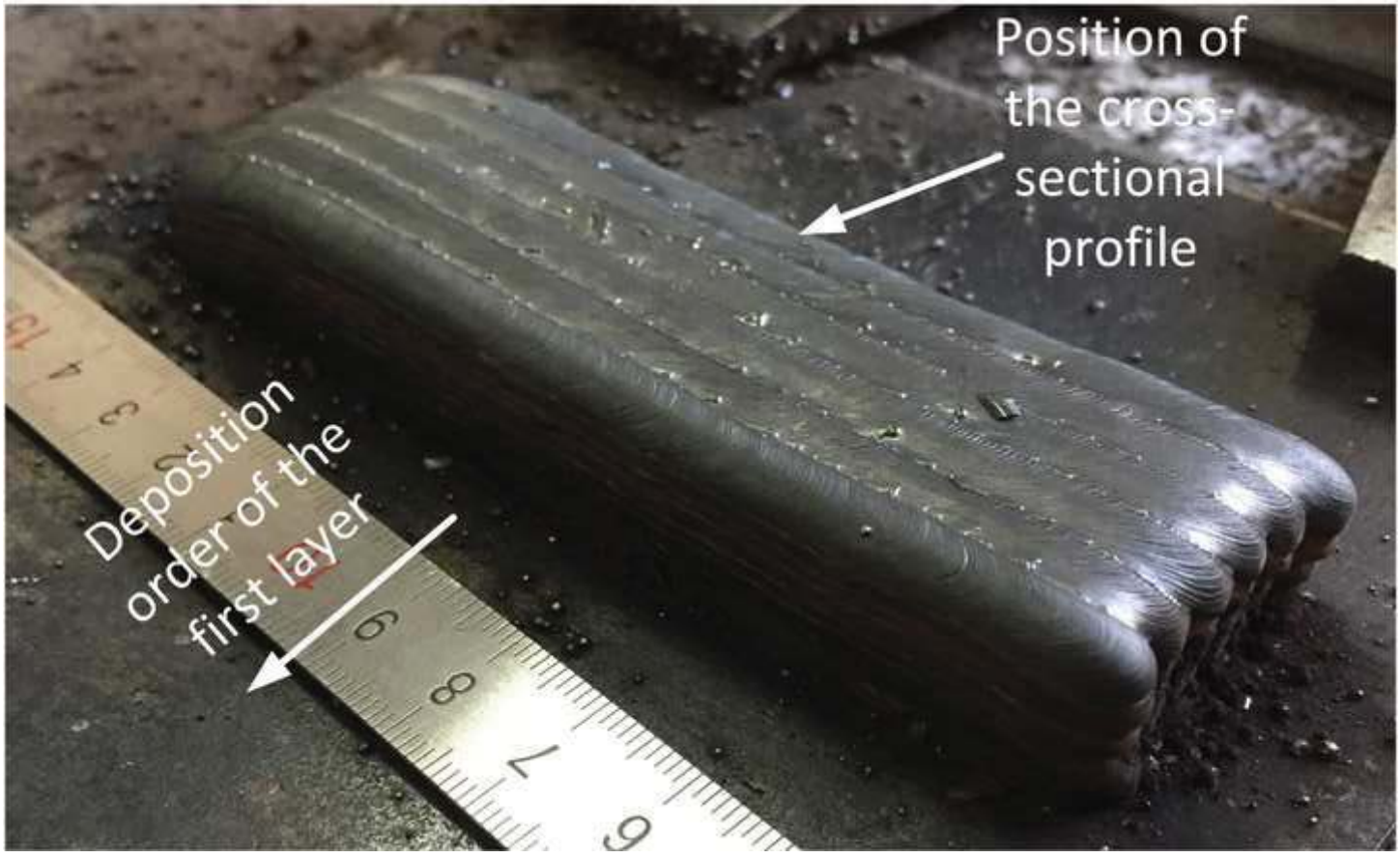

Figure 14b

Click here to download Figure Figure 14b.jpg

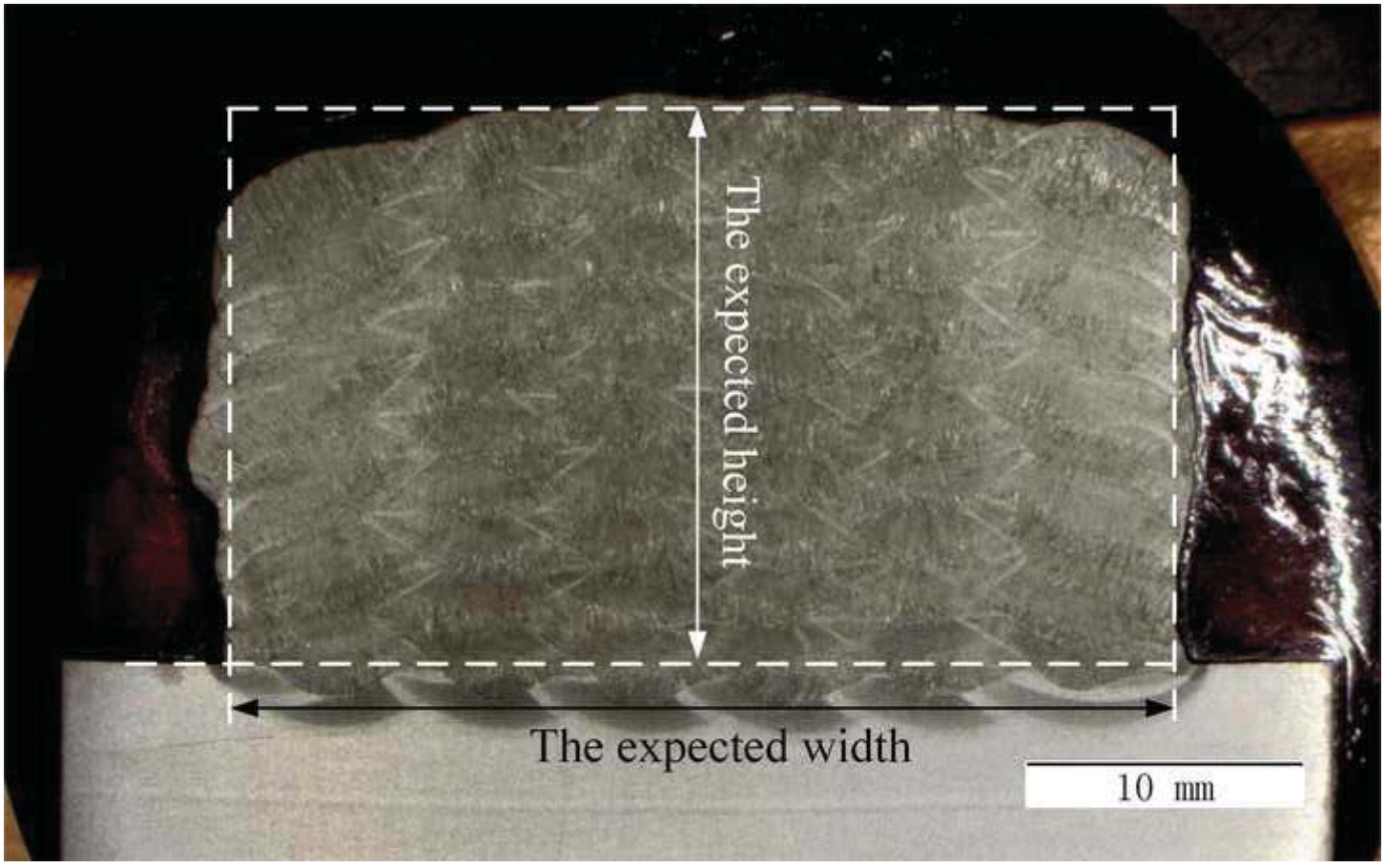

Figure 14c

Click here to download Figure Figure 14c.tif

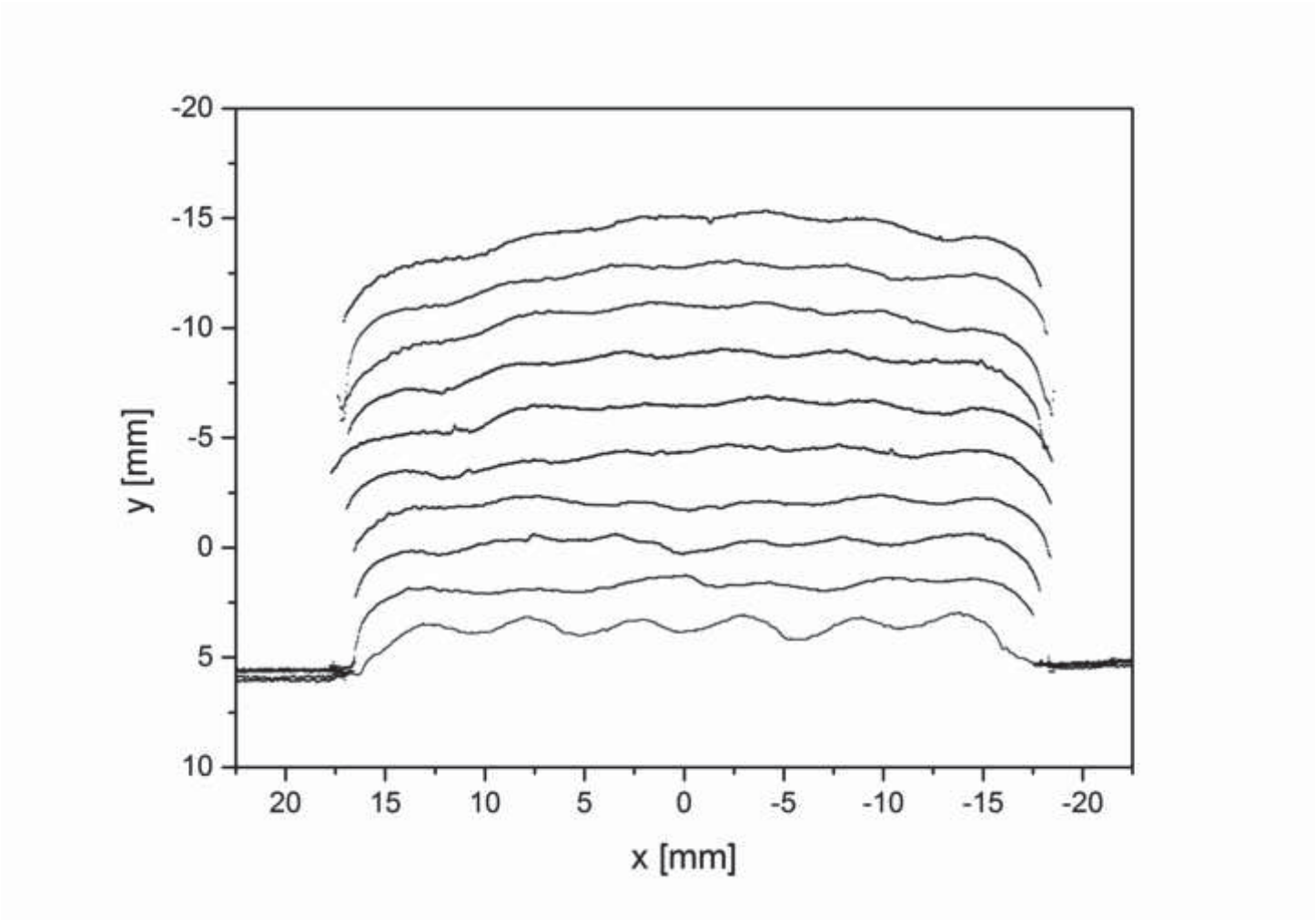

Figure 15

Click here to download Figure Figure 15.jpg

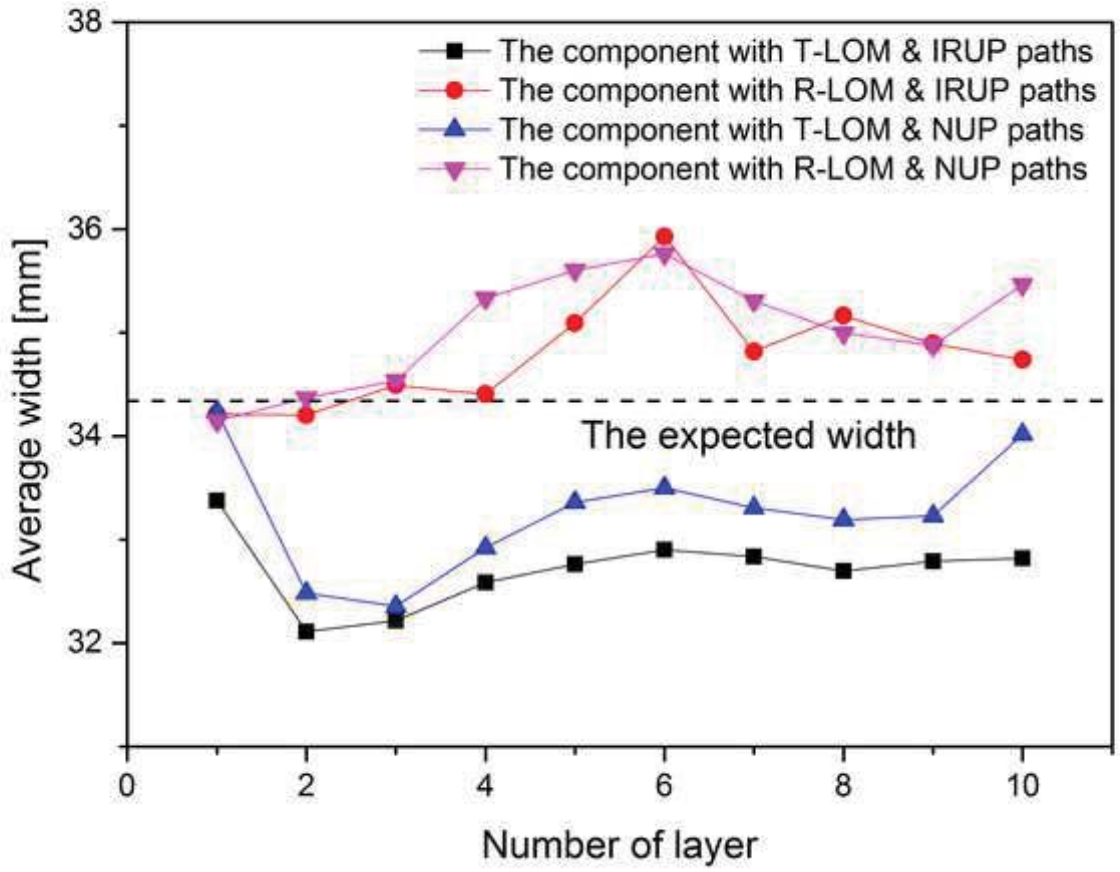

Figure 16a

Click here to download Figure Figure 16a.jpg

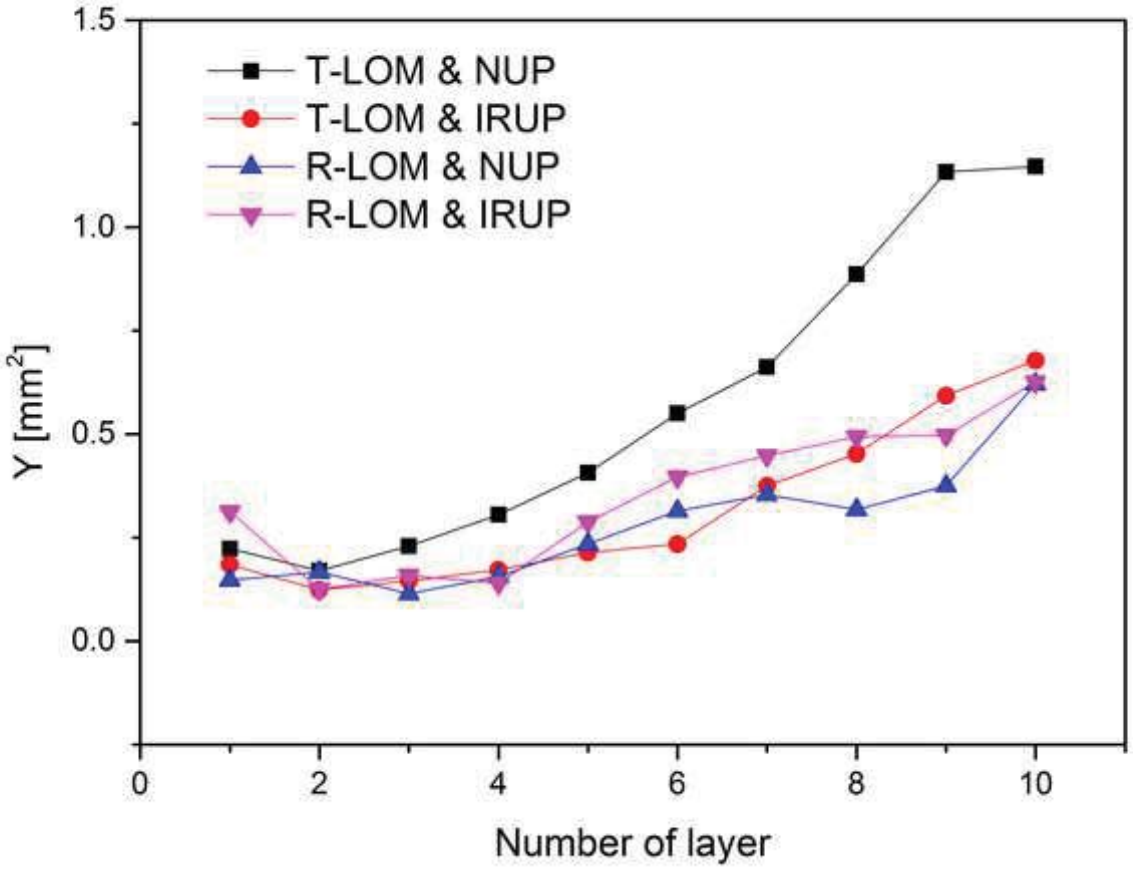

Figure 16b

Click here to download Figure Figure 16b.jpg

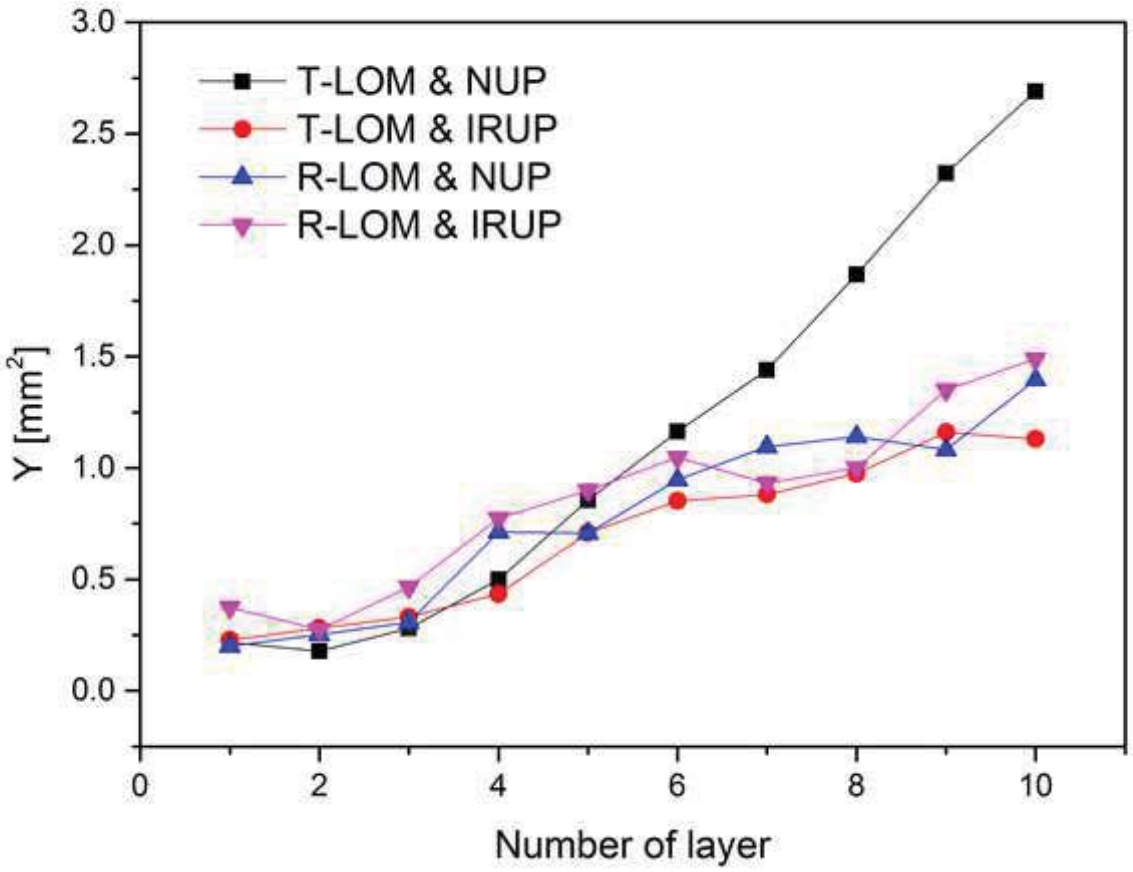

Abbreviations used in the text

Abbr.	Term/Phase
WAAM	wire and arc additive manufacturing
T-LOM	traditional layers-overlapping model
LOS	layers-overlapping strategy
MLMB components	multi-layer multi-bead components
R-LOM	revised layers-overlapping model
$B(i,j)$	the j^{th} bead belonging to the i^{th} layer
EB	elementary bead
NUP path	normal unidirectional parallel path
IRUP path	interlayer-reverse unidirectional parallel path
CUP path	curved unidirectional parallel path
FoS	flatness of the surface
DEH	deviation from the expected height

Table 1 Manufacturing parameters used in the validation experiments

Manufacturing parameters (Unit)	Value
Wire feed rate (m/min)	3.73
Welding voltage (V)	22
Welding current (A)	150
Deposition speed for the EB (mm/s)	6
Width of the EB (mm)	7.327
Height of the EB (mm)	2.304
Step-over rate	0.738
Distance between the centers of adjacent beads (mm)	5.407
Height of a layer (mm)	2.081

Table 2 The average height of the four fabricated components

Conditions	The average height (mm)
T-LOM & NUP paths	19.518
T-LOM & IRUP paths	20.138
R-LOM & NUP paths	19.814
R-LOM & IRUP paths	19.88